frontiers | Frontiers in Bioengineering and Biotechnology

TYPE Original Research
PUBLISHED 25 September 2024
DOI 10.3389/fbioe.2024.1435228

OPEN ACCESS

EDITED BY
Bing Guo,
Harbin Institute of Technology, Shenzhen, China

REVIEWED BY
Stephanie Hurwitz,
University of Pennsylvania, United States
Jing Zhao,
Zhejiang University, China

*CORRESPONDENCE
Eleftherios Terry Papoutsakis,
epaps@udel.edu

RECEIVED 19 May 2024
ACCEPTED 11 September 2024
PUBLISHED 25 September 2024

CITATION
Das S, Thompson W and Papoutsakis ET (2024) Engineered and hybrid human megakaryocytic extracellular vesicles for targeted non-viral cargo delivery to hematopoietic (blood) stem and progenitor cells.
Front. Bioeng. Biotechnol. 12:1435228.
doi: 10.3389/fbioe.2024.1435228

Engineered and hybrid human megakaryocytic extracellular vesicles for targeted non-viral cargo delivery to hematopoietic (blood) stem and progenitor cells

Samik Das[1,2], Will Thompson[1,2] and Eleftherios Terry Papoutsakis[1,2,3]*

[1]Department of Chemical and Biomolecular Engineering, University of Delaware, Newark, DE, United States, [2]Delaware Biotechnology Institute, University of Delaware, Newark, DE, United States, [3]Department of Biological Sciences, University of Delaware, Newark, DE, United States

Native and engineered extracellular vesicles generated from human megakaryocytes (huMkEVs) or from the human megakaryocytic cell line CHRF (CHEVs) interact with tropism delivering their cargo to both human and murine hematopoietic stem and progenitor cells (HSPCs). To develop non-viral delivery vectors to HSPCs based on MkEVs, we first confirmed, using NOD-scid IL2Rγnull (NSG™) mice, the targeting potential of the large EVs, enriched in microparticles (huMkMPs), chosen for their large cargo capacity. 24 h post intravenous infusion into NSG mice, huMkEVs induced a nearly 50% increase in murine platelet counts. PKH26-labeled huMkEVs or CHEVs localized to the HSPC-rich bone marrow preferentially interacting with murine HSPCs, thus confirming their receptor-mediated tropism for NSG HSPCs, and their potential to treat thromobocytopenias. We explored this tropism to functionally deliver synthetic cargo, notably plasmid DNA coding for a fluorescent reporter, to NSG HSPCs both *in vitro* and *in vivo*. We loaded huMkEVs with plasmid DNA either through electroporation or by generating hybrid particles with preloaded liposomes. Both methods facilitated successful functional targeted delivery of pDNA, as tissue weight-normalized fluorescence intensity of the expressed fluorescent reporter was significantly higher in bone marrow than other tissues. Furthermore, the fraction of fluorescent CD117^{+} HSPCs was nearly 19-fold higher than other cell types *within* the bone marrow 72-h following administration of the hybrid particles, further supporting that HSPC tropism is

Abbreviations: CHEV(s), CHRF extracellular vesicle(s); CHMP(s), CHRF microparticle(s); EP, electroporation; EV(s), extracellular vesicle(s); GFP, green fluorescent protein; HSPC(s), hematopoietic stem and progenitor cell(s); huHSPC(s), human hematopoietic stem and progenitor cell(s); huMkEV(s), human megakaryocytic extracellular vesicle(s); MFI, mean fluorescence intensity; miRFP, monomeric (near) infrared red fluorescent protein; Mk(s), megakaryocyte(s); MkEV(s), megakaryocytic extracellular vesicles(s); MkMP(s), megakaryocytic microparticle(s); MkNP(s), megakaryocyte-wrapped nanoparticle(s); MP(s), microparticle(s); muHSPC(s), murine hematopoietic stem and progenitor cells; NSG, NOD-*scid* IL2Rγ^{null}; NTA, Nanoparticle Tracking Analysis; pDNA, plasmid DNA; PMA, phorbol 12-myrsitate 13-acetate; TEM, transmission electron microscopy; TPO, thrombopoietin; WT, wild type.

10.3389/fbioe.2024.1435228

retained when using hybrid particles. These data demonstrate the potential of these EVs as a non-viral, HSPC-specific cargo vehicle for gene therapy applications to treat hematological diseases.

KEYWORDS

hematopoietic stem and progenitor cells (HSPCs), targeted delivery, gene therapy, tropism, megakaryocytes, platelets, HSPC biodistribution, biodistribution

1 Introduction

Effective, targeted cargo delivery to hematopoietic stem and progenitor cells (HSPCs) for gene therapy applications to treat thalassemias and other hematological abnormalities and diseases remains a major unmet need (Nienhuis, 2013; Osborn et al., 2016; Yu et al., 2016). Megakaryocytic extracellular vesicles (MkEVs), which include microparticles (MkMPs) and exosomes (MkExos), are shed from mature, platelet-producing megakaryocytes and contain endogenous RNA that play a role in the differentiation of hematopoietic stem and progenitor cells (HSPC) into megakaryocytes (Figure 1) (Jiang et al., 2014; Kao et al., 2022). We have previously shown that MkEVs [enriched in MkMPs, which are among the most abundant microparticles in circulation (Flaumenhaft et al., 2009)] interact with HSPCs with specificity/tropism and elicit megakaryopoiesis *in vitro*, without the need for the lineage specific growth factor, thrombopoietin (TPO) (Jiang et al., 2014; Jiang et al., 2017; Kao et al., 2022; Thompson and Papoutsakis, 2023a; Thompson and Papoutsakis, 2023b). TPO is the megakaryocytic-lineage specific growth factor that has also a role in regulating the more primitive HSPC compartment. Tropism for, or specificity of targeting of, HSPCs is mediated by specific human MkEVs (huMkEV) receptors (Jiang et al., 2017). We have also demonstrated that huMkEVs induce *de novo* platelet biogenesis following intravenous administration to wild type (WT; Balb/*c*) mice (Escobar et al., 2020). There was an almost 50% increase in platelet count in mice 16 h post huMkEV administration, but a smaller increase was demonstrated 72 h post administration due to huMkEV clearance in WT mice (Escobar et al., 2020). Biodistribution studies suggested that administered huMkEVs preferentially localized in HSPC-rich organs and notably the bone marrow 24-h post huMkEV administration, but fast clearance of huMkEVs in WT mice prevented biodistribution studies beyond 24 h.

To resolve this fast clearance issue and strengthen the conclusion that huMkEV's tropism for HSPCs is preserved *in vivo*, the first goal of these present studies was to use a better murine model instead of WT mice. This was important so that we can deploy huMkEVs, and notably, huMkMPs, which have a large cargo capacity (Kao and Papoutsakis, 2018), to develop non-viral vectors for targeted cargo delivery, including nucleic acids and proteins, to HSPCs for gene therapy and genome editing applications. Such non-viral vectors would also be non-immunogenic if based on autologous cells. EVs

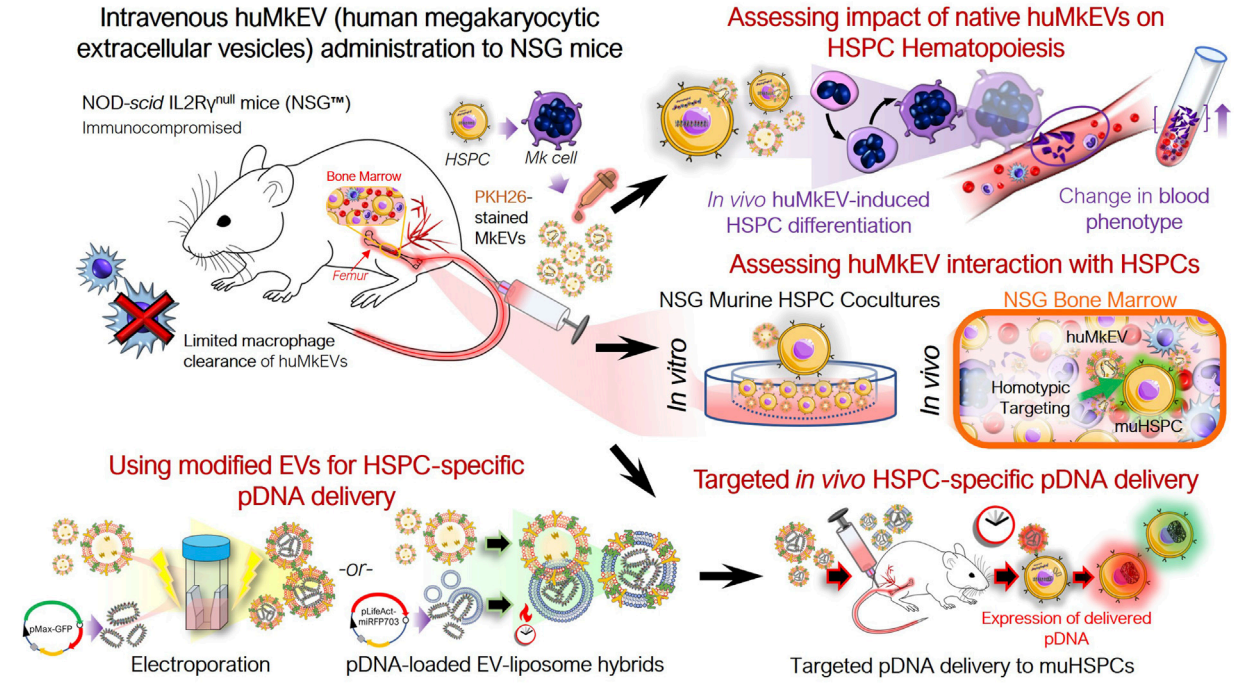

GRAPHICAL ABSTRACT
Graphical Overview: Native and engineered human megakaryocytic extracellular vesicles facilitate targeted non-viral cargo delivery to hematopoietic (blood) stem and progenitor cells.

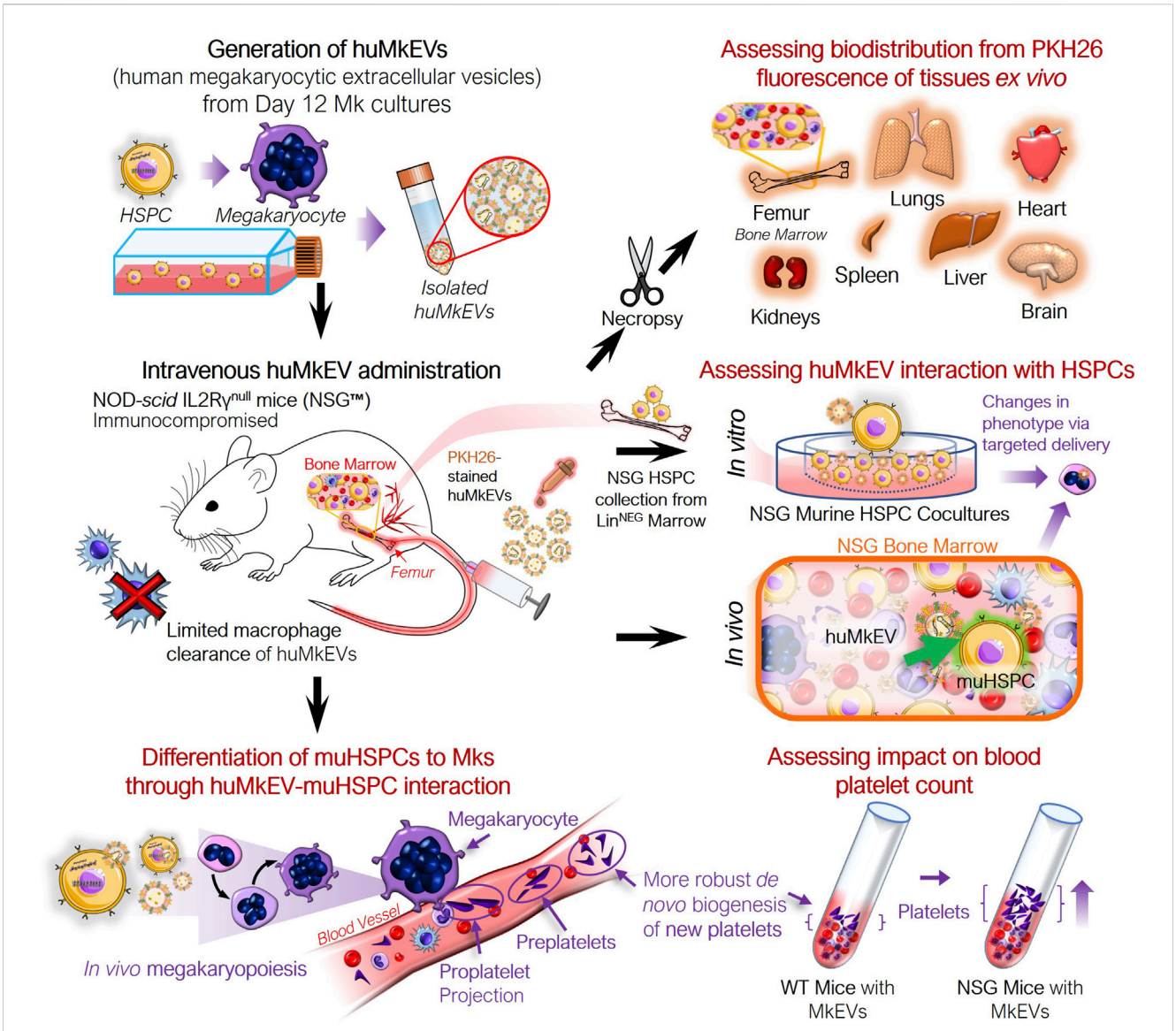

FIGURE 1
Experiment schema for assessing the *in vivo* impact of huMkEVs on NSG™ mice. The NOD-scid IL2Rγ^{null} (NSG™) mouse model was used to determine if the prior observations regarding huMkMP treatment elicit stronger responses in the NSG mice. This particular strain of mice was chosen due to its immunocompromised state devoid of functional macrophages, which could allow for prolonged exposure to huMkMPs due to extended circulation times.

are dynamically exchanged between cells and, through targeted delivery of their cargo, are critical for determining the fate of the target cell following their uptake (de Jong et al., 2019; Belliveau and Papoutsakis, 2022; Kao et al., 2022; Belliveau and Papoutsakis, 2023). Thus, we hypothesized that by loading native EVs or modified EVs such as the EV hybrids discussed in this study, we can *functionally* deliver with specificity/tropism for HSPCs, plasmid DNA, both *in vitro* and *in vivo*. The goal would be to demonstrate their potential for targeted therapy of genetic hematological disorders.

Given the fast clearance of huMkEVs in WT mice, the immunodeficient NOD-*scid* IL2Rγ^{null} (NSG™) mouse model offered the best option for our studies (Strowig et al., 2011; Wang et al., 2015; Brehm et al., 2019). NSG mice is one of the most widely used immunocompromised murine strains for engraftment with human hematopoietic cells and other human cells or tissues. As NSG mice are largely devoid of functional macrophages, we hypothesized that the administered huMkEVs would reside longer in circulation and/or in murine tissues compared to immunocompetent WT mice (Serreze et al., 1993; Rodriguez et al., 2013; Brehm et al., 2019). If the administered huMkEVs do remain in the murine system for an extended period of time, we hypothesized that the response to infused huMkEVs will be magnified in comparison to WT mice. Additionally, due to the hypothesized longer retention of the infused huMkEVs in circulation, the NSG model may also better showcase the versatility of huMkEVs as a targeted drug delivery platform for nucleic acids and other cargo. Finally, given their smaller size, NSG mice can be administered a smaller effective EV dose than other rodent models (e.g., rats), thus increasing the scope and practicality of our studies. Producing large quantities of EVs is time consuming

and expensive in the academic setting (Thompson and Papoutsakis, 2023a; Thompson and Papoutsakis, 2023b).

As NSG mice exhibit aberrant hematopoiesis such as lower frequencies of myeloid lineage cells (which include megakaryocytes) compared to other humanized mice, a first goal is to test the hypothesis that huMkEVs interact with murine NSG HSPCs to induce *in vitro* megakaryopoiesis and thrombopoiesis as with WT murine HSPCs (Saito et al., 2020). As such, our data from WT mice (Escobar et al., 2020) provide no guidance as to what would occur with NSG HSPCs. To demonstrate that huMkEVs interact with murine NSG HSPCs to induce *in vitro* megakaryopoiesis and thrombopoiesis, we examined if coculture of huMkEVs with murine NSG HSPCS results in higher numbers of murine platelets (PLTs), pre and proplatelets (PPTs), megakaryocytes (Mks), and MkEVs. Following positive outcomes from the *in vitro* studies, our second goal was to examine if huMkEVs also induce *in vivo* megakaryopoiesis and thrombopoiesis and if they demonstrate tropism in interacting with murine NSG HSPCs.

The success of these *in vitro* and *in vivo* studies using NSG mice suggested that huMkMPs could be the basis for developing non-viral vectors for cargo delivery to murine HSPCs. Thus, a third goal was to examine if huMkMPs loaded via electroporation (Kao and Papoutsakis, 2018) with plasmid DNA coding for a fluorescent report could deliver the plasmid to murine HSPCs, both *in vitro* and *in vivo*, the latter with tropism, to demonstrate fluorescent protein expression. Because electroporation (Kao and Papoutsakis, 2018) results in low yields of loaded huMkEVs, and may also affect the levels of receptors (Jiang et al., 2017) that enable target specificity/tropism towards, and cargo delivery to, HSPCs, a fourth goal was to examine if a recently reported method for loading pDNA via the formation of hybrid liposome-huMkEV nanovesicles can be successfully deployed for functional delivery of pDNA to murine NSG HPSCs, both *in vitro* and *in vivo* (Jiang et al., 2017; Lin et al., 2018).

We have already extensively characterized the large huMkEVs (i.e., huMkMPs) produced from our specific cell culture and isolation protocols as recently summarized (Thompson and Papoutsakis, 2023b). These characterizations fulfill the requirements outlined by the International Society for Extracellular Vesicles (Thery et al., 2018).

2 Materials and methods

2.1 Material sourcing

All materials were purchased from Thermo Fisher Scientific or Millipore-Sigma unless otherwise noted. All cytokines were ordered from PeproTech Inc.

2.2 Preparation of huMkEVs from primary CD34 cells and CHRF EVs (CHEVs) from PMA-treated CHRF-288 cells

Human megakaryocytic extracellular vesicles (huMkEVs) were generated from Day 12 cultured megakaryocytes deriving from primary human $CD34^+$ HSPCs using the protocols detailed by Panuganti et al. (2013). Briefly, $CD34^+$ from different healthy donors (Fred Hutchinson Cancer Center) were pooled and cultured in a serum-free medium, namely, IMDM medium containing 20% BIT9500 serum substitute (STEMCELL) supplemented with human LDL and a cytokine cocktail tailored to induced megakaryopoiesis (recombinant human thrombopoietin (TPO), stem cell factor (SCF) IL-3, IL-6, IL-9, and IL-11). On Day 7, $CD61^+$ megakaryoblasts were enriched from the culture via MACS using anti-CD61 magnetic microbeads (Miltenyi Biotec), and the selected cells were re-cultured into flasks containing IMDM, BIT9500, TPO, SCF, and nicotinamide. On Day 12, MkEVs were isolated by first pelleting out any cells and debris at 2,000 × g for 10 min, and the supernatant was ultracentrifuged at 25,000 × g for 30 min at 4°C to collect the MkEVs.

Following isolation of the huMkEVs, the EV pellet was resuspended in 500 µL Diluent C and combined with a mix of 500 µL Diluent C and PKH26 dye (Puzar Dominkus et al., 2018). After 5 min of incubation at ambient temperature, the EV suspension was quenched with 1.5 mL of 3% BSA (bovine serum albumin) solution, and the stained EVs were ultracentrifuged at 25,000 × g for 30 min at 4°C, followed by a second wash with 1X PBS. The PKH26-stained huMkEVs were resuspended in 100 µL 1X PBS and stored at −80°C prior to the *in vitro* cocultures and intravenous administration to mice.

To prepare CHRF EVs (CHEVs), CHRF-288 cells were expanded in CHRF media containing IMDM, 10% (v/v) heat-inactivated fetal bovine serum (FBS), 3.023 g/L $NaHCO_3$ (sodium bicarbonate), and 1% (v/v) 100x antibiotic-antimycotic (αα), and incubated at 37°C, 20% O_2, 5% CO_2, and 85% relative humidity (rH) (Fuhrken et al., 2007). To induce a megakaryocytic phenotype, CHRF cells were re-cultured in CHRF media supplemented with 1.5 ng/L of phorbol 12-myrsitate 13–6 acetate (PMA), seeded at a density of 3–4 × 10^5 cells/mL, and incubated at 37°C for 3 days (Fugman et al., 1990; Konkle et al., 1992). On Day 3, cells and debris were pelleted from the treated culture at 2,000 × g for 10 min, and EVs were isolated from the supernatant using the protocol used for isolating huMkEVs.

2.3 Preparation of NSG HSPCs for *in vitro* cocultures

To collect lineage-negative HSPCs from NSG mice, femurs from untreated NSG mice were collected and stored in tissue storage buffer comprising of RPMI 1640X buffer supplemented with 10% (v/v) heat-inactivated fetal bovine serum (FBS) and 1% (v/v) 100x antibiotic-antimycotic (αα) as described by Madaan et al. (2014). Next, muscles, connective tissues, and fat were cleared from the femur bones, and the cleaned bones were washed with 1X PBS containing 1% (v/v) αα and placed on a Petri dish. After cleaning, the epiphyses were sliced from each end of the femur, and 3-mL of tissue storage buffer was flushed through the femur using a 20G needle equipped syringe to evacuate the bone marrow; the bone fragments were gently crushed to release more marrow. Finally, the evacuated marrow was transferred to a conical tube through 30 µm pre separation filter (Miltenyi Biotec) to collect the marrow cells.

To isolate the NSG HSPCs from the flushed bone marrow, the evacuated marrow cells were first pelleted at 300 × g for 10 min, and

the marrow cells were resuspended in ACK (ammonium-chloride-potassium) buffer (Escobar et al., 2020) to lyse any red blood cells (RBCs). After lysing, the RBC-depleted marrow cells were washed multiple times with PBS. Next, the pelleted marrow cells were incubated with direct lineage cell magnetic microbeads as described by Escobar et al. (2020) (Miltenyi Biotec), and the lineage-negative NSG HSPCs were collected after MACS depletion of the lineage-positive marrow cells. After several washes with IMDM, the isolated NSG HSPCs were prepared in co-culture media (80% IMDM, 20% BIT9500, 100 ng/mL SCF, 1% v/v αα) and incubated at 37°C (20% O_2, 5% CO_2, and 85% rH) until re-culturing.

2.4 Exogenous loading of huMkEVs with plasmid DNA

3.2 μg of pMax-GFP pDNA (Lonza) was labeled with Cy5 (Mirus) and premixed with 5×10^6 CHEVs and resuspended in up to 100 μL hypo-osmolar buffer; the pDNA-EV premix was transferred to a 2-mm electroporation cuvette and incubated at 37°C for 15 min. After incubation, the pDNA-EV-loaded cuvettes were electroporated at 200 V, 100 mA and immediately placed on ice. Next, the electroporated EVs were centrifuged at 1,000 × g for 10 min to remove any agglomerates, and the pDNA-loaded EVs were isolated from the supernatant following centrifugation at 25,000 × g for 30 min at 4°C. Finally, the pDNA-loaded EVs were resuspended in a small volume of filtered 1X PBS and stored at −80°C until use.

To prepare the pDNA-loaded liposome-EV hybrids, pLifeAct-miRFP703 was first loaded into liposomes (Lipofectamine 2000) using the protocol adapted from Thermo Fisher (Shcherbakova et al., 2016). Briefly, 1 μg of pDNA and 2 μL of the Lipofectamine 2000 reagent were each diluted in 25 μL IMDM each. Next, each diluted aliquot was mixed, and the 50 μL mix was incubated at room temperature for 5 min. To hybridize the pDNA-loaded liposomes with PKH26-stained CHEVs, the hybridization protocol developed by Lin et al. (2018) was adopted and modified. After preparing the 50 μL pDNA-liposome complexes, 5×10^6 EVs were dosed into each mix and incubated at 37°C for 12 h. Following incubation, the CHEV-liposome hybrids were stored at 4°C until use. Separately, 50 μL liposome complexes were prepared with 1 μg of pDNA and 2 μL of Lipofectamine 2000 as an additional liposome-only control condition.

To characterize the liposomes, CHEVs, and CHEV-liposome hybrids, samples were diluted in Millipore-filtered water, and three technical replicates of each diluted sample was measured using nanoparticle tracking analysis (NTA; Malvern NanoSight NS300). The particle size distribution was calculated using the NanoSight NS300 software. To measure the zeta potential, approximately 350 μL of each sample was loaded into an Anton Paar Omega cuvette, and three technical replicates were measured using the Litesizer 500 (Anton Paar). To quantify plasmid DNA loading efficiency, the loaded liposomes and CHRF EV-liposome hybrids were pelleted at 25,000 × g for 30 min at 4°C, and the pellets were resuspended in lysis buffer (Qiagen); the supernatants were retained to quantify 'free' or unloaded pDNA. Next, the lysate and supernatant were applied to pDNA binding columns, washed with PE wash buffer (Qiagen), and eluted using biology-grade water. Final pDNA concentration was determined using the Qubit DNA quantification kit (Invitrogen). TEM (transmission electron microscopy) images were prepared by the University of Delaware Bioimaging Center as described (Belliveau and Papoutsakis, 2022).

2.5 Coculture of huMkEVs with isolated NSG HSPCs and ploidy, platelet counts

After collecting the NSG muHSPCs from the femurs of untreated mice, muHSPCs were cultured in media containing 80% (v/v) IMDM, 20% (v/v) BIT9500, 1% antibiotic-antimycotic, and 100 ng/mL rhSCF and incubated at 37°C with 20% O_2, 5% CO_2, and 85% rH for 24 h. The following coculture conditions were used:

i) Untreated control: ~7.5×10^4 muHSPCs in 750 μL of coculture media only (80% IMDM, 20% BIT9500, 100 ng/mL rhSCF, 1% αα)
ii) +rhTPO: ~7.5×10^4 muHSPCs in 750 μL of coculture media supplemented with 100 ng/mL rhTPO
iii) +huMkEVs: ~7.5×10^4 muHSPCs in 750 μL of coculture media incubated with 30:1 (huMkEVs: muHSPCs), or 2.25×10^6 PKH26-stained huMkEVs

Following 5 days of incubation at 37°C, 50 μL of each culture was incubated with FITC rat anti-mouse CD41a, APC rat anti-mice CD117, or APC rat anti-mice CD45 to measure levels of murine megakaryocytes, stem and progenitor cells, and non-erythrocyte differentiated hematopoietic cells, respectively. Fractions of $CD41a^+$, $CD45^+$, and $CD117^+$ cells were gated against unstained controls. Following CD41a staining, platelets were counted via flow cytometry (BD FACSAria II) using FSC-SSC gating previously optimized for counting platelets in RBC-lysed murine peripheral blood (Escobar et al., 2020). Total platelet concentration was determined after diluting 10 μL of AccuCount beads (Spherotech), which were used as a standard.

To quantify the ploidy of megakaryocytes, the protocol of Lindsey and Papoutsakis (2011) was used. Briefly, mature megakaryocytes were fixed with 4% paraformaldehyde in 1X PBS for 15 min at room temperature and subsequently permeabilized with 70% methanol for 1 h at 4°C. Next, the permeabilized megakaryocytes were stained with FITC rat anti-mouse CD41a and the nuclei were further stained with 50 μg/mL propidium iodize to gauge ploidy. Finally, ploidy was assessed via flow cytometry, with ploidy counts determined from DNA content through the distinct peaks of propidium iodide fluorescence.

To assess the degree of megakaryopoiesis of the Day 5 cultures via confocal microscopy, each culture was immunostained for β1-tubulin (TUBB) and von Willebrand factor (VWF), which are highly abundant in platelets and critical for platelet adhesion, and thus, characteristic of mature megakaryocytes (Sadler, 2005; Cuenca-Zamora et al., 2019). Briefly, 100 μL of each culture was seeded onto poly-L-lysine coated coverslips, fixed with 4% paraformaldehyde in 1X PBS, and blocked with blocking buffer (1X PBS, 10% normal donkey serum, 3% bovine serum albumin) for 1 h at room temperature. Next, the coverslips were incubated with a

1:100 dilution of rabbit anti-VWF (Abcam) and 1:100 mouse anti-TUBB in blocking buffer at room temperature for 2 h. After washing with PBS, each coverslip was subsequently incubated with a 1: 1,000 dilution Alexa Fluor 488 anti-rabbit IgG and 1:1,000 Alexa Fluor 647 anti-mouse IgG_3 κ at room temperature for an additional 2 h. Finally, the immunostained coverslips were sealed onto glass slides with SlowFade mounting media with DAPI, sealed with nail polish, and stored at 4°C until imaging.

2.6 Coculture of pDNA-loaded huMkEVs and CHEVs with NSG HSPCs *in vitro* for assessment of HSPC-specific cargo delivery

To assess the efficiency of using electroporated huMkEVs to deliver pMax-GFP pDNA, the following cocultures were set up:

i) Untreated control: ~1.0 × 10^5 muHSPCs in 750 µL of coculture media only (80% IMDM, 20% BIT9500, 100 ng/mL rhSCF, 1% αα)
ii) pDNA electroporation: ~1.0 × 10^5 muHSPCs electroporated with 1 µg pMax-GFP pDNA in 750 µL of coculture media
iii) +pDNA-loaded huMkEVs: ~1.0 × 10^5 muHSPCs cultured with 3 × 10^6 pDNA-loaded huMkEVs (30:1 huMkEV: muHSPC) in 750 µL of coculture media

Following treatment, 50 µL of each sample and replicate were collected after 6, 24, 48, and 72 h of incubation and measured for GFP fluorescence via flow cytometry (BD FACSAria II) and gated against untreated controls.

To assess the efficiency of using CHEV-liposome hybrids to deliver pLifeAct-miRFP703 pDNA, the following cocultures were set up:

i) Untreated control: ~1.0 × 10^5 muHSPCs in 750 µL of coculture media only (80% IMDM, 20% BIT9500, 100 ng/mL rhSCF, 1% αα)
ii) +Liposomes: ~1.0 × 10^5 muHSPCs incubated with 50 µL containing 1 µg pLifeAct-miRFP703 liposome complexes in 750 µL of coculture media
iii) +CHRF EV-liposomes: ~1.0 × 10^5 muHSPCs cultured with 50 µL CHRF EV-liposome hybrids containing 1 µg pDNA in 750 µL of coculture media

To measure pDNA uptake and expression, 50 µL samples were collected after 6-, 24-, 48-, and 72-h of incubation and measured for miRFP703 fluorescence using flow cytometry (Beckman CytoFLEX S). miRFP703-fluorescent populations were gated against untreated controls to exclude background fluorescence.

To prepare samples for screening via confocal microscopy, 100 µL of each 72-h culture was seeded onto poly-L-lysine coverslips, fixed, and washed as described above. Next, to label the cell cytoskeleton, each coverslip was incubated with 500 µL filtered PBS containing 5 µL Alexa Fluor 488-conjugated phalloidin and incubated at room temperature for 1 h. Finally, the prepared coverslips were washed with PBS, mounted onto slides with SlowFade mounting media with DAPI, and sealed with nail polish. Slides were stored at 4°C until imaging via confocal microscopy (Zeiss LSM 880).

2.7 Administration of huMkEVs and collection of various tissues from NSG mice for biodistribution analysis

Prior to administering huMkEVs to the NSG mice, PKH26-stained huMkEVs were thawed, immunostained with FITC-conjugated mouse IgG anti-human CD41a (BD Lifesciences) and counted via flow cytometry (BD FACSAria II). Next, aliquots containing 5 × 10^6 huMkEVs were each resuspended in 150 µL sterile filtered PBS and loaded into sterile 50 cc insulin syringes. After preparing the huMkEV samples, 6–8-week-old female NSG mice were briefly warmed and were administered with either 150 µL sterile PBS only or with 5 × 10^6 huMkEVs in PBS via the tail vein. The mice were then grouped by treatment and housed in a sterile environment until necropsy and analysis 4, 24, 48, or 96 h following treatment.

After euthanasia using CO_2 asphyxiation and cervical dislocation, the femurs, heart, lungs, spleen, liver, kidneys, and brain were excised and placed in 3 mL of cold tissue storage buffer (RPMI 1640X with 10% v/v FBS) (Madaan et al., 2014). Next, each tissue was trimmed of any connective tissue and fat and rinsed with 1X PBS containing 1% αα (v/v). After rinsing and weighing, each tissue was placed in 2 mL bead mill homogenizer tubes containing 1 mL hypotonic lysis buffer and 2.8 mm ceramic beads (90 mg/bead; 6x beads/tube). To homogenize the tissues, each tube was loaded into a bead mill homogenizer (Fisher Bead Mill 24) and homogenized at 5.0 m/s for 20 s with four total cycles. The bone marrow was extracted from the femurs and processed without lineage depletion as described above, and the final bone marrow flushes were resuspended in 1-mL tissue storage buffer until analysis.

To measure PKH26 biodistribution, 2 × 200 µL of each tissue homogenate was loaded into an opaque-bottomed 96-well plate and checked for fluorescence (λ_{excit}: 551 nm, λ_{em}: 567 nm) using a microplate reader (SpectraMax i3x). Tissue autofluorescence was accounted for by subtracting the mean fluorescence of each tissue from PBS-only treated mice. After tabulating the net tissue mean fluorescence intensity, fluorescence values were normalized by the tissue weight of each individual tissue.

2.8 Preparation of murine blood for platelet counts and phenotypic analysis

Prior to euthanasia and necropsy, approximately 100–200 µL of murine blood was extracted via cardiac puncture and collected in a K2-EDTA microtainer (BD Lifesciences). Next, 10 µL of the chelated blood was drawn into a capillary tube and placed in 990 µL ammonium oxalate RBC lysis buffer. After RBC lysis, 100 µL of the depleted blood was incubated with 2.5 µL FITC rat anti-mouse CD41a at 4°C for 15 min to immunostain and identify megakaryocytes, platelets, pre and proplatelets, and megakaryocytic microparticles via flow cytometry.

To quantify total platelet counts per unit of blood through flow cytometry (BDFACSAria II), 10 µL of AccuCount fluorescent beads (Spherotech) was added to each depleted blood sample following CD41a antibody incubation. Next, platelets and pre/proplatelets were gated on CD41a+ populations using FSC-SSC gating previously optimized for counting platelets in murine blood in

wild-type mice. Total platelet concentration was calculated using the known concentration of the AccuCount beads as a standard, and final counts were adjusted for the initial dilution in RBC lysis buffer.

2.9 Intravenous administration of pDNA-loaded CHRF EVs to NSG mice to determine *in vivo* cargo delivery to murine HSPCs

Prior to intravenous administration, PKH26-labeled huMkEVs and CHEVs were loaded with pMax-GFP and pLifeAct-miRFP703, respectively, as described above. Next, several aliquots of 6×10^6 of the electroporated huMkEVs were resuspended 150 µL PBS; separate 5 µg aliquots of Cy5-labeled pMax-GFP were prepared in 150 µL PBS to serve as an additional control. After preparing the samples, 6–8-week-old female NSG mice were intravenously administered with either PBS only, pDNA, or pDNA-loaded huMkEVs via the tail vein, and all treated mice were grouped by their treatment condition and housed in a sterile environment for 24 h.

Next, the treated mice were euthanized, and each tissue sample was homogenized and loaded into microplates as described above. Microplates were then measured for both PKH26 and GFP (λ_{excit}: 475 nm, λ_{em}: 509 nm) fluorescence to assess the huMkEV biodistribution and GFP expression, respectively. As before, tissue autofluorescence within both spectra was accounted for by subtracting the raw fluorescence of each tissue collected from PBS-treated mice. RBC-depleted bone marrow samples were seeded, fixed, and blocked onto poly-L-lysine coated coverslips as described above. Coverslips were subsequently immunostained with Alexa Fluor 594-conjugated rat IgG2b anti-mouse CD117 to label HSPCs and incubated for 2 h at room temperature. Finally, the coverslips were mounted onto glass slides with SlowFade mounting media with DAPI, sealed, and stored at 4°C until imaging.

To treat NSG mice with the CHEV-liposome hybrids, the protocol described above was scaled to prepare doses comprised of 45×10^6 PKH26-stained CHEVs and 9 µg pLifeAct-miRFP703 in 250 µL IMDM media as prepared. An equivalent amount of pDNA was complexed with liposomes as an additional control. Next, mice were intravenously administered via the tail vein with either 250 µL IMDM (negative control), pDNA-loaded liposome complexes, or pDNA-loaded CHEV-liposome hybrids. Mice were then grouped by their experimental condition and housed in a sterile environment for 72 h until necropsy.

Following necropsy, tissues were homogenized and prepared as described previously. Next, PKH26 (λ_{excit}: 551 nm, λ_{em}: 567 nm) and miRFP703 (λ_{excit}: 670 nm, λ_{em}: 703 nm) fluorescence were measured via a microplate reader (SpectraMax i3x) were assessed to determine CHEV-hybrid biodistribution and pDNA expression, respectively; the raw autofluorescence of the IMDM-only treated mice was subtracted for each tissue in each of these respective channels. Net fluorescence values were subsequently normalized by the tissue weights. Blood platelet counts were estimated through flow cytometry (Beckman CytoFLEX S) as described in previous sections.

Femurs from the treated mice were flushed and RBC-lysed as described in Section 2.2. Next, flushed bone marrow cells were seeded onto poly-L-lysine coverslips, fixed, and initially blocked as described in Section 2.10. To label murine HSPCs, coverslips were immunostained with a 1:100 dilution (in blocking buffer) of rat IgG2b anti-mouse CD117 for 2 h at room temperature. Next, the primary antibody-stained coverslips were secondarily stained with a 1:1,000 dilution of Alexa Fluor 594-conjugated anti-rat for an additional 2 h at room temperature. After immunostaining and washing, each coverslip was mounted on glass slides with SlowFade mounting media with DAPI, sealed, and stored at 4°C until imaging.

2.10 Immunostaining bone marrow cells and select tissues for phenotype analysis via flow cytometry and confocal microscopy

Following necropsy, marrow cells were extracted from the femurs using the protocol outlined above without any lineage depletion. After collecting the marrow cell flushes, each flush was resuspended in an equivalent volume of tissue storage buffer, and approximately 50 µL of each suspension was retained for flow cytometry immunostaining prior to lysis. Next, to assess the fraction of murine megakaryocytes and HSPCs in the bone marrow, 50 µL aliquots of marrow cells were immunostained with 5 µL Alexa Fluor 488-conjugated rat IgG1 anti-mouse CD41 or APC-Cy7-conjugated rat IgG2b anti-mouse CD117 (BioLegend) and incubated at 4°C for 15 min. The immunostained marrow cells were next analyzed via flow cytometry (BD FACSAria II). Positively immunostained populations were gated against unstained controls. To determine uptake of huMkEVs by the marrow cells, cells were also analyzed for PKH26 fluorescence.

To prepare samples for confocal microscopy, RBCs were depleted from the flushed marrow cells by resuspending the bone marrow cells in ACK buffer for 5 min. Next, the RBC-depleted bone marrow cells were washed 2–3 times with 1X PBS at 300 × g for 10 min. After pre-coating each coverslip with 200 µL 0.1% poly-L-lysine for at least 30 min and washing, 100 µL of each bone marrow sample was seeded, fixed onto coverslips, and blocked with blocking buffer using the protocol described above. Next, the fixed cells were immunostained with a 1:100 dilution of rabbit anti-CD41 and rat IgG2a anti-Sca-1 (Abcam) in blocking buffer to identify murine megakaryocytes and HSPCs, respectively. After incubating with the primary antibody mix for 2 h at room temperature, each coverslip was stained with a secondary 1:1,000 dilution of Alexa Fluor 488-conjugated anti-rabbit and Alexa Fluor 647-conjugated anti-rat for an additional 2 h at room temperature. Finally, following several washes with PBS, each coverslip was sealed onto glass slides with SlowFade mounting media with DAPI, sealed with nail polish, and stored at 4°C until imaging.

For histological tissue analysis and immunofluorescence staining, samples collected from 4- and 24-h huMkEV treated mice were processed at the Nemours Histology Core facility (Wilmington, DE). Samples collected from NSG mice treated with the pDNA-loaded liposomes and CHEV-liposomes were processed at the University of Delaware Histology Core facility (Newark, DE). Briefly, femurs, lungs, liver, spleen, and kidneys were fixed with 10% neutral-buffered formalin for several days. Next, after decalcification of the femur, tissues were imbedded in paraffin, sectioned, mounted on slides, and deparaffinized prior to immunostaining.

For the prepared samples collected from the huMkEV-only treated mice (and PBS control), sectioned tissues were immunostained with rabbit anti-mouse CD41 and rat IgG2b anti-mouse Sca-1 to label murine megakaryocytes and HSPCs, respectively; cell nuclei were stained with DAPI. The immunostained tissues were secondarily stained with Alexa Fluor 488 anti-rabbit and Alexa Fluor 647 anti-rat, to label $CD41^+$ and $Sca\text{-}1^+$ cells, respectively. Finally, the prepared samples were imaged via confocal microscopy (Zeiss LSM 880).

For the samples collected from mice treated with pDNA-loaded liposomes or CHEV-liposome hybrids, each sectioned tissue was either immunostained with rabbit anti-mouse CD41 -or- rat IgG2b anti-mouse Sca-1 to label murine megakaryocytes and HSPCs, respectively. The immunostained tissues were secondarily stained with Alexa Fluor 488 anti-rabbit -or- Alexa Fluor 405 anti-rat, to label $CD41^+$ and $Sca\text{-}1^+$ cells, respectively. Finally, the prepared samples were imaged via confocal microscopy (Invitrogen EVOS M7000 and Zeiss LSM 880).

2.11 Statistical analysis

For *in vitro* experiments, statistical analysis was calculated via a Student's t-test. For all animal/*in vivo* experiments, analysis of variance (ANOVA) was used for all statistical analyses and comparisons. Significance was denoted with *N.S.: not significant, *: $p < 0.1$, **: $p < 0.05$, ***: $p < 0.01$*, and *****: $p < 0.001$* unless otherwise noted. Error bars are shown as ± standard error of the mean.

3 Results

3.1 *In vitro* studies: huMkEVs effectively interact to deliver their native cargo to NSG murine HSPCs as demonstrated by their ability to induce *de novo* megakaryopoiesis and platelet biogenesis

As interaction with and huMkEV cargo delivery to HSPCs is receptor mediated (Jiang et al., 2017), and because NSG mice have aberrant hematopoiesis [notably in erythroid and granulocytic lineages (Cao et al., 1995; Reya, 1996; Yurino et al., 2016)], it could not be predicted *a priori* that their HSPCs (mu^{NSG} HSPCs) will interact with huMkEVs. Thus, prior to *in vivo* studies, it was necessary to test that huMkEVs interact and deliver their cargo to mu^{NSG} HSPCs by culturing huMkEVs with mu^{NSG} HSPCs (Figure 1). To collect mu^{NSG} HSPCs, femurs were collected from untreated female NSG mice ($n = 3$), and bone marrow cells were isolated and subsequently lineage-depleted via MACS (Miltenyi Biotec) to collect uncommitted mu^{NSG} HSPCs and cultured as described in the methods, at a ratio of 30 huMkEVs per mu^{NSG} HSPC, a ratio that was based on our prior work (Escobar et al., 2020). At Day 5, each culture was immunostained for murine CD41a, CD45, and CD117, and differentiation into megakaryocytic lineage was further tested via immunostaining cultured cells for presence of β1-tubulin (TUBB1) and von Willebrand factor (VWF), both of which are characteristic of mature platelets and megakaryocytes (McGrath et al., 2010; Jiang et al., 2014; Cuenca-Zamora et al., 2019).

Using flow cytometry, both rhTPO and huMkEV treatment resulted in significant increase in the fraction of $CD41a^+$ cells (Figure 2A) over the untreated control. Furthermore, huMkEV treatment yielded higher ploidy $CD41a^+$ cells (Figure 2B), indicating the development of more mature megakaryocytes in culture (Ravid et al., 2002). Both rhTPO-treated and huMkEV-treated cultures generated significantly higher counts of murine megakaryocytes, but less than 20% of the megakaryocytes from rhTPO-treated cultures exhibited ≥4N ploidies as opposed to nearly 40% of megakaryocytes from huMkEV-treated cultures exhibiting high (≥4N) ploidies (Figure 2C). This was further confirmed after measuring the platelet counts in each culture using $CD41a^+$ staining and FSC-SSC gates optimized previously for WT mice blood platelet analysis; we observed a nearly 40-fold higher platelet count and 4-fold higher pre/proplatelet count with the huMkEV-treated cultures over each other condition (Figure 2D). Finally, using confocal microscopy, we observed that huMkEV-treated HSPCs visibly expressed both von Willebrand factor (vWF) and β1-tubulin (TUBB1) following 5 days of treatment, which assist with platelet coagulation and are found almost exclusively on platelets and mature megakaryocytes (Figure 2E). These data support the hypothesis that, *in vitro*, huMkEVs effectively interact with and deliver their native cargo to mu^{NSG} HSPCs.

3.2 Intravenous administration of huMkEVs to NSG mice increases murine megakaryocyte and platelet biogenesis

Next, we examined if huMkEV-induced megakaryopoiesis of muHSPCs could result in *de novo* platelet biogenesis *in vivo* across a series of timepoints (Figures 1, 3A). The goal of these murine experiments was to demonstrate that huMkEVs deliver their cargo to murine HSPCs, and for that, we used platelet formation as an *in vivo* assay that shows delivery of the huMkEV cargo to muHSPCs. This *in vivo* delivery assay is based on our prior findings where we have shown that RNA and notably microRNAs in the huMkEVs induce megakaryopoiesis of HSPCs in the absence of TPO (Jiang et al., 2017; Kao et al., 2022). The ability of MkEVs to induce *de novo* megakaryopoiesis *in vivo* was demonstrated in our 2020 Blood Advances paper (Escobar et al., 2020). For these experiments, each mouse was administered 150 µL dose of either prediluted 6×10^6 PKH26-stained huMkEVs ($n = 26$ mice) or saline (PBS) solution ($n = 15$ mice) (Supplementary Table S1). The dose of huMkEVs was chosen based on our experiments with WT mice (Escobar et al., 2020) as it did not adversely affect WT mice, yet it may be suboptimal for lack of resources to carry out a dose study in these laboratory experiments, which is not an issue for clinical applications as the technology to manufacture EVs and notably huMkEVs is reasonably well established (Estes et al., 2022; Thompson and Papoutsakis, 2023a; Thompson and Papoutsakis, 2023b). The large number of mice engaged in this study was in order to examine four time points (4, 24, 48 and 96 h) as each mouse is sampled at one time point only. Each dose was administered intravenously via tail vein injection. Mice were handled and kept in an aseptic environment until euthanasia. To count platelets, blood was drawn and collected from each mouse via cardiac puncture immediately prior to euthanasia. After the red blood cells were lysed,

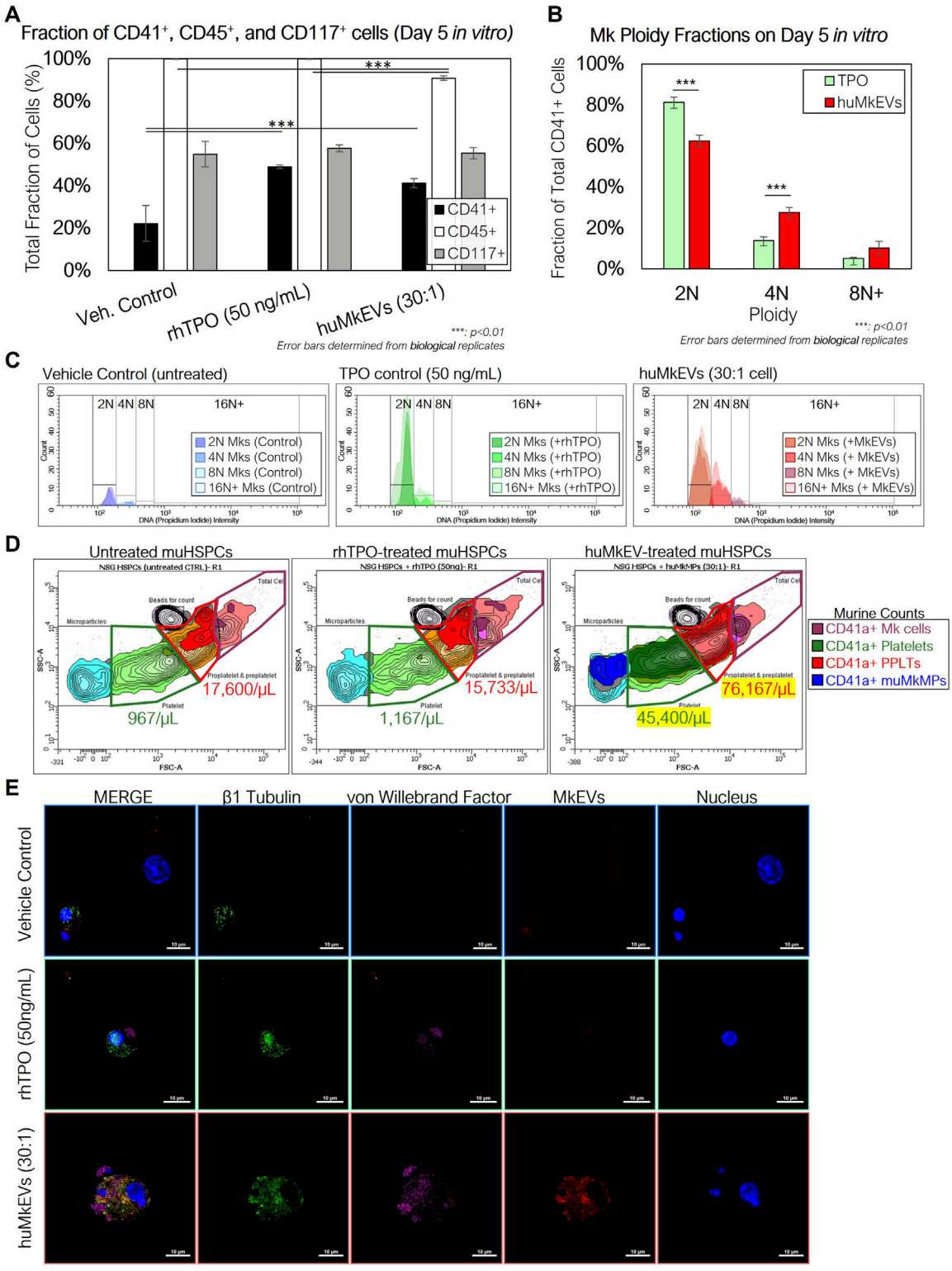

FIGURE 2
Coculture of NSG™ murine HSPCs with huMkEVs *in vitro* induces more effective megakaryopoiesis than treatment with thrombopoietin (TPO) alone. Murine HSPCs were extracted and pooled from a set of three female NSG™ mice, and were cultured in media containing IMDM, BIT, and 100 ng/mL stem cell factor (SCF) under the following conditions: 1) no treatment (control) 2) treatment with 50 ng/mL of rhTPO, and 3) treatment with a 30:1 ratio of PKH26-stained huMkEVs per cell. **(A)** After 5 days, each culture was stained for murine CD41a, CD45, and CD117 and measured via flow cytometry to assess megakaryopoietic differentiation of murine HSPCs in each condition. **(B)** Cells from each condition were permeabilized and stained with CD41a and DAPI and measured with flow cytometry to determine megakaryocytic ploidy. **(C)** Total count-normalized histograms depicting DNA (propidium iodide) intensity of CD41a+ murine Mks from control (blue-shaded; left), rhTPO-treated (green-shaded; middle), and huMkEV-treated (red-shaded; right) (*Continued*)

FIGURE 2 (Continued)
conditions. **(D)** Platelets, pre- and proplatelets, and microparticles were counted using calibrated fluorescent beads (1×10^6 beads/mL) and forward scatter (FSC), side scatter (SSC) gates set from previous wild type murine blood counts. Lighter colors correspond to a higher density of particles, while darker colors correspond to lower densities. **(E)** The untreated (top row), TPO-treated (middle row) and huMkEV-treated (bottom row) cultures were immunostained for β1 tubulin (green; second column) and von Willebrand factor (violet; third column) to determine the degree of differentiation of the murine HSPCs to the megakaryocytic phenotype. Scale bars: 10-μm. **: $p < 0.1$, **: $p < 0.05$, ***: $p < 0.01$, ****: $p < 0.001$, Student's t-test.*

we measured the concentration of murine CD41a$^+$ platelets (PLTs) and pre/proplatelets (PPLTs) via flow cytometry.

There were notable differences in PLT counts between the saline-treated and huMkEV-treated mice at both 24- and 48-h after treatment (Figure 3B). We observed a significant 50% boost in PLT counts in the huMkEV-treated mice after 24-h; while still significant, the relative PLT boost diminished to 30% at 48-h (Figure 3B). PPLT counts were more variable and boosts in huMkEV-induced PPLT counts were limited to 48-h following treatment (Figure 3C). Differences in platelet counts subsided 96-h following treatment, possibly indicating a return to steady-state NSG murine hematopoiesis. One would note that even the control injection of PBS (Figures 3B, C) resulted in an increase in platelets and pre/proplatelets. This is because injection PBS alone is sufficient to induce inflammation in mice and inflammation increases platelet formation. While indeed PBS increases platelet formation, injection of MkEVs result in higher levels of platelet formation. PBS controls are to account for the inflammation induced platelet formation.

As we observed a significant increase in platelet counts after 24 h, we wanted to determine the relative fractions of CD41a$^+$ (Mk) cells and Sca-1/CD117$^+$ murine HSPCs within the bone marrow. Sca-1 is more abundantly expressed on both hematopoietic stem and progenitor cells than the more primitive CD117 marker (Visnjic et al., 2004; Nadri et al., 2007; Jindal et al., 2014). We flushed out and RBC-depleted the marrow from the excised NSG femurs, and after several washes with PBS, the collected marrow was stained for CD41a$^+$ and CD117$^+$ cells. Relative fractions of muHSPCs in the marrow were similar at 4- and 24-h following treatment, but muHSPC fractions at 48-h were nearly 30% higher in the huMkEV-treated marrow than that of the saline-treated control (Figure 3D). CD41a$^+$ cell fractions followed a different trend, with a short-term relative boost in CD41a$^+$ counts measured at 24-h in the huMkEV-treated marrow followed by a significant drop at 48-h (Figure 3E). Interestingly, the relative drop in CD41a$^+$ marrow cells in the huMkEV-treated mice coincides with the boost in platelet counts at 48 h, and might reflect the maturation of murine megakaryocytes and subsequent generation of platelets. This trend was confirmed via confocal microscopy, with visibly greater numbers of large polyploid megakaryocytes in the marrow of huMkEV-treated mice at 24 h (Supplementary Figure S2). The differences were not as notable at 48 or 96 h (Supplementary Figure S2).

3.3 The NSG murine model enables more conclusive huMkEV biodistribution data

As the huMkEVs were pre-stained with PKH26, a strong yellow-orange lipophilic dye, PKH26 fluorescence of the excised and homogenized tissues was used to estimate huMkEV localization and biodistribution. While PKH26 labeling may increase the size of EVs (Forteza-Genestra et al., 2021), such an increase in size would improve detection of the labeled EVs and EV uptake via flow cytometry and microscopy. From this assessment, the bone marrow, liver, and kidneys, exhibited immediate (4-h) increases in mean fluorescence intensity (MFI) from the PKH26-stained huMkEVs (Figure 4A). When accounting for the mass of each tissue, the bone marrow exhibited the greatest increase in PKH26 MFI after 24 h, amounting to one of the highest MFI levels per normalized tissue mass. Notably, the magnitude of the mean fluorescence intensity of PKH26 in nearly all of the tissues examined was nearly 10–20-fold higher in NSG mice in comparison to their WT counterparts (Escobar et al., 2020). Blood and the NSG bone marrow continued to exhibitcomparatively high weight-normalized PKH26 fluorescence at 48 and 96 h following treatment (data not shown) The fluorescence persistence at 48 and 72 h in the blood does not mean that whole MkEVs persist that long in circulation, although they likely persist longer in NSG mice than in WT mice (Escobar et al., 2020). The persisting fluorescence in blood means that the fluorescence from MkEVs is transferred to HSPCs (Jiang et al., 2017), which then produce progenitor cells and more mature cells that go into circulation while carrying the fluorescence that originated from labeled huMkEVs.

Immunostaining the various tissues with murine CD41a and Sca-1 also helped us determine if the huMkEVs preferentially localized to these specific cell types (CD41a$^+$ or Sca-1$^+$ cells) within the tissue. As we have previously reported, huMkEVs targets and induces the megakaryocytic differentiation of not only the most primitive hematopoietic stem cells but also early progenitor cells (Jiang et al., 2014). As Sca-1 is more abundantly expressed on both hematopoietic stem and progenitor cells than the more primitive CD117 marker (Visnjic et al., 2004; Nadri et al., 2007; Jindal et al., 2014), using Sca-1, we can visualize a broader set of colocalization events with physiologically important HSPCs in tissues. After 24-h, we observed high degrees of colocalization between the PKH26-fluorescent huMkEVs and the Sca-1$^+$ murine HSPCs lining the femoral bone marrow (Figure 4B). The frequency of murine HSPCs was lower in the other screened tissues, such as the lungs (Figure 4C), liver (Figure 4D), spleen (Figure 4E), and kidneys (Figure 4F), but there was a strong degree of colocalization between huMkEVs and murine HSPCs in the spleen, lungs, and kidneys. huMkEVs were localized to the tubules within the kidney (Figure 4F), which are a particularly enriched with Sca-1$^+$ cells (Vanderijn et al., 1989; Cray et al., 1990; Blake et al., 1993; Holmes and Stanford, 2007). Both huMkEVs and Sca-1 cells were at their highest density in the

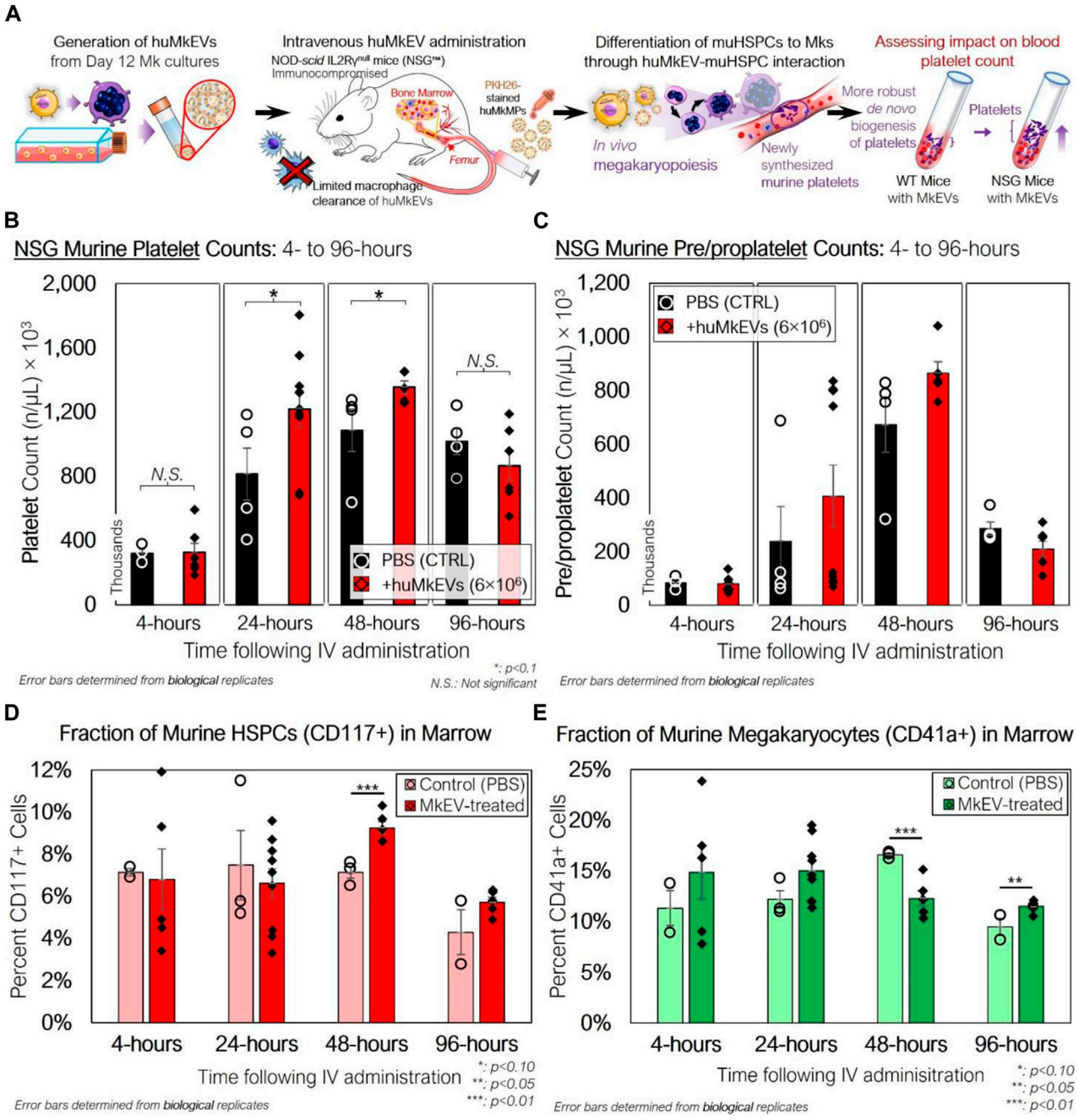

FIGURE 3
Peripheral blood platelet, pre/proplatelet, and microparticle counts and bone marrow phenotype of NSG mice treated with huMkEVs. **(A)** Experiment schema for assessing the *in vivo* impact of huMkEVs on megakaryopoiesis in NSG™ mice. **(B)** Platelets and **(C)** pre/proplatelets from RBC-depleted peripheral blood were counted using calibrated fluorescent beads (1×10^6 beads/mL), murine CD41a staining, and forward scatter (FSC), side scatter (SSC) gates set from previous wild type murine blood counts. All values are shown as count, in thousands, per μL blood. Dashed (PBS) and solid (huMkEV) lines show average counts and trends across each timepoint. n: 3, 4, 4, four for PBS-treated mice and n: 6, 9, 5, 6 for huMkEV-treated mice at 4-, 24-, 48-, and 96-h, respectively. **(D)** Murine $CD117^+$ HSPCs and **(E)** $CD41a^+$ megakaryocyte -cell fractions of flushed, RBC-depleted femoral bone marrow as determined via flow cytometry. *: $p < 0.10$, **: $p < 0.05$, N.S.: not significant. Analysis of Variance (ANOVA) was used for statistical comparisons for all animal experiments.

periphery of the blood vessels within the vasculature of the bone marrow, which is a one of the most HSPC-rich regions of bone marrow (Itkin et al., 2016). These data demonstrate that, *in vivo*, huMkEVs retain their tropism for murine HSPCs, thus demonstrating the potential of using huMkEVs as vectors for targeted delivery of genetic cargo to HSPCs.

3.4 *In vitro* and *in vivo* functional plasmid DNA delivery to murine HSPCs using engineered huMkEVs

We have previously shown that plasmid DNA (pDNA) can be successfully loaded into huMkEVs via electroporation, and the

10.3389/fbioe.2024.1435228

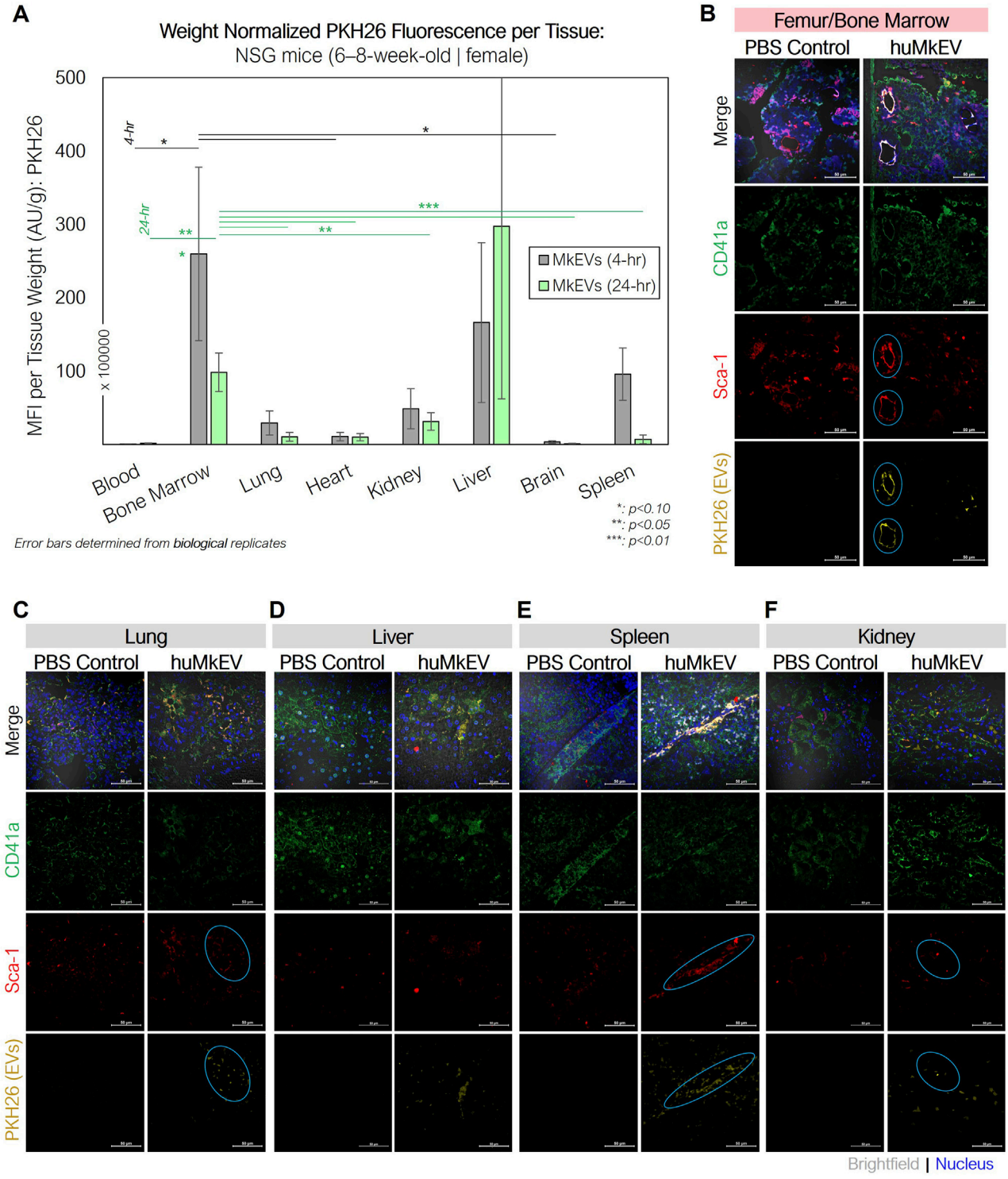

FIGURE 4
huMkEV biodistribution (MFI: AU/g) in various excised tissues and immunofluorescence assessment of bone marrow following huMkEV intravenous administration to NSG mice. **(A)** Normalized mean fluorescence intensity (MFI) from each homogenized tissue reveals that huMkEVs localize to kidney, RBC^+ bone marrow 4- and 24-h following administration. Overall, with increasing time post administration of huMkEVs, PKH26 MFI decreases in most tissues except for peripheral blood, which shows increased MFI with increasing time. 24-h post treatments, murine tissues from **(B)** femurs, **(C)** lungs, **(D)** livers, **(E)** spleens, and **(F)** kidneys were fixed (10% neutral-buffered formalin), sectioned, immunostained and assessed for structure (gray- DIC) and presence of $CD41^+$ cells (green), $Sca\text{-}1^+$ cells (blue), and PKH26 fluorescence arising from administered huMkEVs. Colocalization of PKH26 fluorescence with either $CD41^+$ or $Sca\text{-}1^+$ cells is shown in white-orange in the merged image and circles in teal in their respective channels. Scale bars: 50-μm. **: $p < 0.1$, **: $p < 0.05$, ***: $p < 0.01$.* Analysis of Variance (ANOVA) was used for statistical comparisons for all animal experiments.

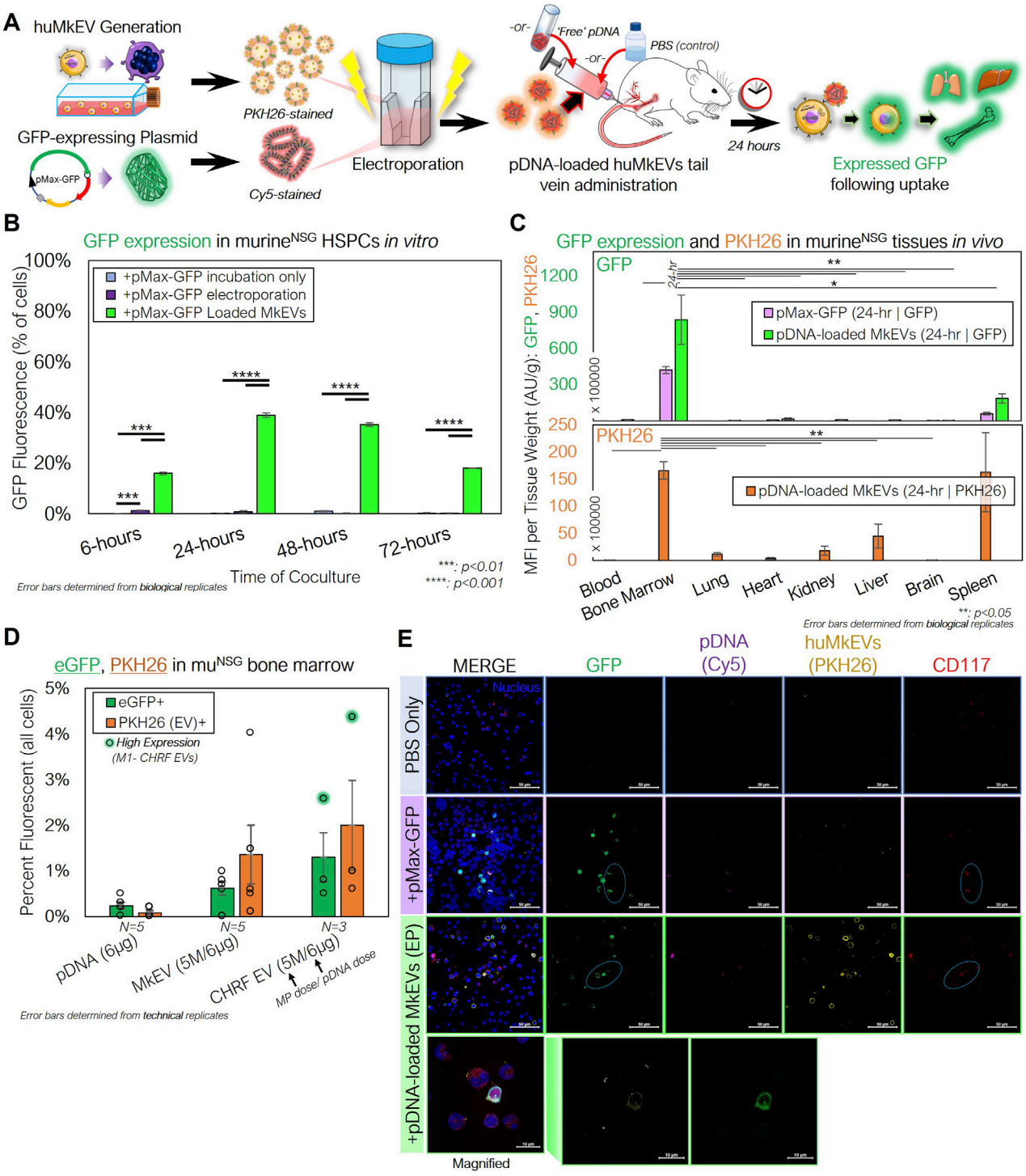

FIGURE 5
huMkEVs and CHRF EVs (CHEVs) can be electroporated with plasmid DNA for HSPC-specific nucleic acid delivery. **(A)** Experimental schema for preparing pMax-GFP-loaded huMkEVs via electroporation for targeted pDNA delivery to murine HSPCs *in vitro* and *in vivo*. **(B)** HSPCs from NSG mice were cultured with either 'free' pDNA (pMax-GFP), directly electroporated with pDNA, or cocultured with huMkEVs loaded via electroporation with pDNA, and assessed for GFP expression. **(C)** 6×10^6 pDNA-loaded huMkEVs via electroporation or an equivalent amount of 'free' pDNA were intravenously administered to NSG mice ($n = 2$, each condition), and tissues were excised, homogenized, and assessed for GFP (top) and PKH26 fluorescence (bottom; huMkEV-treated only) after 24-h of treatment. **(D)** Flushed marrow cells from mice treated either with 'free' pDNA, pDNA-loaded huMkEVs, or pDNA-loaded CHEVs were assessed for GFP and PKH26 fluorescence using flow cytometry; background fluorescence was accounted for from data of untreated (PBS) mice. **(E)** Flushed RBC-depleted marrow cells from the two pDNA conditions and a PBS-treated control were immunostained for $CD117^+$ HSPCs (red) and screened for GFP (green), Cy5-stained pDNA (purple), and huMkMPs (yellow). Colocalization of murine HSPCs and GFP indicated with cyan circles and nuclei are shown in blue. Scale bars: 50-μm. Magnified inset shows distinct PKH26 and GFP puncta within flushed marrow cells from pDNA-loaded huMkEV-treated mice. Scale bars: 10-μm. *: $p < 0.1$, **: $p < 0.05$, ***: $p < 0.01$, ****: $p < 0.001$. Student's t-test was used for in vitro experiments. Analysis of Variance (ANOVA) was used for statistical comparisons for all animal experiments.

pDNA-loaded huMkEVs can functionally delivered to human HSPCs ($CD34^+$ cells) *in vitro* (Kao and Papoutsakis, 2018). Functional delivery was demonstrated by showing delivery of the pDNA to the huHSPC nucleus, and by low level expression of the plasmid encoded green fluorescence protein (GFP). Delivery to WT or NSG murine HSPCs either *in vitro* or *in vivo* has not been examined.

To test first *in vitro* delivery, we cultured lineage-depleted murine HSPCs collected from untreated NSG mice femurs with PKH26-stained huMkEVs loaded via electroporation with Cy5-labeled pDNA expressing for GFP (pMax-GFP) (Figure 5A). Within 24 h of incubation, nearly 40% of the NSG HSPCs expressed GFP, indicating both successful delivery and functional expression of the pDNA. This expression sustained for 48 h following incubation but subsided after 72 h (Figure 5B).

For *in vivo* studies, we intravenously administered prediluted 6×10^6 PKH26-stained huMkEVs loaded with Cy5-dyed pMax-GFP via electroporation (n = *2* mice). As a control, two mice were also treated with a dose of 'free' pDNA, which was equivalent to the total amount of pDNA electroporated into the huMkEVs. After 24-h, murine tissues (bone marrow/femurs, lungs, hearts, kidneys, liver, brain, spleen, and blood) were excised, homogenized, and analyzed for GFP fluorescence. We observed that only the flushed femoral bone marrow and spleen contained GFP fluorescence following either pDNA alone or pDNA-loaded huMkEV treatment, with the marrow containing significantly higher GFP fluorescence than any other analyzed tissue (Figure 5C). PKH26 fluorescence, which is also a measure of localization and biodistribution of the administered huMkEVs, followed a similar biodistribution pattern (Figure 5C).

Similar effectiveness was demonstrated when we analyzed bone marrow cells collected from NSG mice treated with an equivalent amount of pDNA-loaded CHEVs, which are EVs generated from cultured human CHRF-288 cells, a fast growing megakaryoblastic cell line (Figure 5D). We had shown previously (Jiang et al., 2017) the importance of surface markers (such as ICAM-1/CD54 and MAC-1) expressed in huMkEVs for enabling the specificity of targeting HSPCs. These molecules are also expressed on the CHRF cell line and in fact at higher levels compared to primary megakaryocytes (Das et al., 2023), which could suggest greater expression of these surface molecules on CHEVs than huMkEVs. Upon further analysis of the flushed bone marrow cells, we observed that the huMkEV- or CHEV-delivered pDNA resulted in greater GFP expression than pDNA alone (Figure 5D). Additionally, after immunostaining the flushed bone marrow cells for CD117, confocal microscopy revealed colocalization between murine HSPCs and GFP (Figure 5E) in mice treated with either pDNA alone or pDNA-loaded huMkEVs.

While these results demonstrated the potential of huMkEVs as a vehicle for HSPC-specific nucleic acid delivery, the low yield of electroporation-loaded EVs due to EV agglomeration prompted us to explore other methods for loading cargo into huMkEVs. Lin *et al.* developed a method of producing hybrid pDNA-loaded liposome HEK293 EV hybrids for delivering pDNA to hard-to-transfect mesenchymal stem cells (Lin et al., 2018; Li et al., 2022). We thus constructed miRFP703-expressing pDNA-loaded liposome-CHRF EV hybrids (CHEV hybrids; Figure 6A). Nanoparticle tracking analysis (NTA) of the loaded hybrid particles indicated a ~57-nm increase in the mean diameter over the unmodified CHRF EVs (Figure 6B). A change in morphology was also observed via transmission electron microscopy (TEM; Figure 6C). Additionally, the zeta potential of the CHEV hybrids fell between that of the CHEVs and the liposomes, further indicating hybridization between the two types of vesicles (Figure 6D). Greater than 90% of the pDNA was loaded into both the liposomes and the CH EV-liposome hybrids, indicating efficient encapsulation of the pDNA payload (Figure 6E).

After 24 h of incubating CHEV hybrids with NSG HSPCs, nearly 40% of the cocultured HSPCs expressed miRFP703 (Figure 6F). This fraction was similar to the earlier *in vitro* coculture with the electroporated EVs at 24 h (Figure 5B), but the fraction of fluorescent cells continued to climb at 48 and 72 h with the CHEV hybrid-treated muHSPCs. Greater than 90% of the $miRFP703^+$ HSPCs at 24, 48, and 72 h were also $PKH26^+$, indicating that the expressed pDNA was delivered via the CHEV hybrid system (Figure 6G). This expression was further confirmed via confocal microscopy (Figure 6H), with both liposome- and CHEV hybrid-treated muHSPCs exhibiting robust miRFP703 expression within the cell cytoplasm.

After confirming successful delivery of and expression from the miRFP703 plasmid *in vitro*, we used pDNA-loaded CHEV hybrids to assess targeted pDNA delivery *in vivo* (Figure 7A). As a control, unhybridized pDNA-loaded liposomes were prepared using the same amount of pDNA (10 μg). An equivalent volume of IMDM was prepared as an additional control. 72-h following treatment, murine tissues were excised and analyzed for PKH26 and miRFP703 fluorescence.

In assessing the biodistribution of the CHEV hybrids, the tissue-mass normalized PKH26 fluorescence revealed a different pattern compared to our previous biodistribution studies using either unloaded huMkEVs or electroporated pDNA-loaded huMkEV-treated mice (Figures 4A, 5C), as fluorescence was almost exclusively limited to the peripheral blood and bone marrow (Figure 7B). The magnitude of PKH26 fluorescence in the peripheral blood was also 5-fold higher than the blood from huMkEV-only treated mice at any prior assessed timepoint (Figures 4A, 5C, 7B). This may indicate that the CHEV hybrids may circulate in the blood for extended time periods, thus explaining their limited localization in other tissues. As the PKH26 fluorescence was largely limited to the blood and bone marrow, miRFP703 was exclusively limited to the bone marrow in both the liposome and CHEV hybrid-treated mice (Figure 7B). The persisting fluorescence in blood was of the same origin as that in the data of Figure 4A. Unlike the use of huMkEVs (Figure 3), there were no significant changes in platelet and pre/proplatelet counts between the control and either liposome- or CHEV hybrid-treated mice (Supplementary Figures S3A, S3B). This suggests possible dilution or loss of some of the native EV cargo (which is responsible for inducting the megakaryocytic differentiation of HSPCs) in the CHRF EVs following hybridization with the liposomes and/or differences in the endogenous cargo between MkEVs and CHEVs (Jiang et al., 2017; Kao et al., 2022).

Further analysis of the flushed bone marrow cells revealed that the CHEV hybrids retained their tropism to HSPCs *in vivo*. After immunostaining the marrow cells for murine CD117 and CD41, we found that the fraction of miRFP703 fluorescent cells was comparatively higher in murine HSPCs ($CD117^+$ cells) and megakaryocytes ($CD41^+$ cells) compared to other marrow cells and to the liposome only control; PKH26 from the CHEV hybrids also

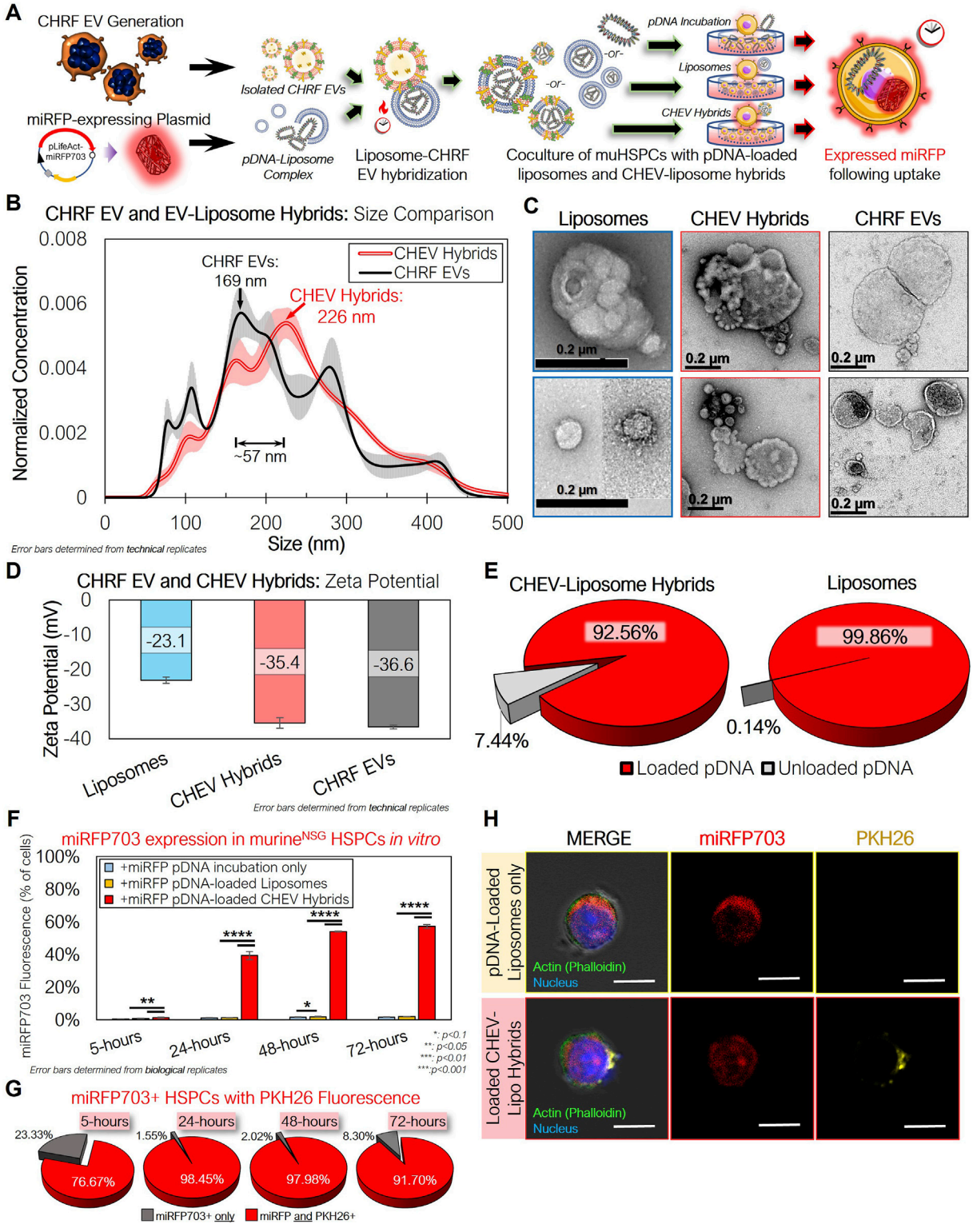

FIGURE 6
CHRF EVs (CHEVs) can be loaded with plasmid DNA via hybridization with pDNA–loaded liposomes and can be used for efficient *in vitro* nucleic acid delivery to murine HSPCs. **(A)** Experimental schema for preparing pLifeAct-miRFP703-loaded liposomes or CHEV-liposome hybrids for targeted pDNA delivery to murine HSPCs *in vitro*. **(B)** Nanoparticle tracking analysis (NTA) of isolated CHEVs and CHEV-liposome hybrids showing an increase in diameter following hybridization. **(C)** TEM images of loaded liposomes, CHEV-liposome hybrids (CHEV hybrids), and CHEVs. Scale bars: 0.2-µm/200-nm. **(D)** Zeta potential of liposomes, CHEV hybrids, and CHEVs. **(E)** Fraction of pDNA retained within the liposome or hybrid particles. **(F)** Isolated NSG HSPCs were incubated with either 'free' (unloaded) pDNA expressing far-red miRFP703, pDNA-loaded liposomes, or pDNA-loaded CHEV hybrids and assessed for miRFP703 expression. **(G)** Fraction of miRFP703$^+$ HSPCs also exhibiting PKH26 fluorescence, indicating pDNA delivery via CHEV hybrids. **(H)** Actin-
(*Continued*)

FIGURE 6 (Continued)
stained (green) HSPCs from 96-h cultures were screened for miRFP703 (red) and PKH26 fluorescence from pre-stained CHEVs to assess the presence of CHEV hybrids (yellow). *: $p < 0.1$, **: $p < 0.05$, ***: $p < 0.01$, ****: $p < 0.001$, N.S.: not significant. Student's t-test was used for all in vitro experiments.

preferentially localized to $CD41^+$ and $CD117^+$ cells over other marrow cells (Figure 7C). The high miRFP703-expressing mouse, an outlier, was given the same dose, but it showed much higher miRFP703 expression. The liposome-only delivery is a measure of expression level without specific targeting, and one should consider the possibility that the clearance of loaded liposomes is slower than the clearance of the loaded hybrid particles, as these hybrids contain human membranes and proteins. While the biodistribution data suggest that both the loaded liposomes and CHEV hybrids were both successful at delivering the miRFP703 plasmid to the marrow (Figure 7B), the higher fraction of miRFP703 expressing-HSPCs demonstrate that targeting of muHSPCs by CHEV hybrids is retained. The flushed marrow cells also exhibited distinct PKH26 and miRFP703 fluorescent puncta under confocal microcopy, further confirming successful delivery of the pDNA to the marrow (Supplementary Figure S4).

To further probe if there were any distinct colocalization patterns between miRFP expression and murine HSPCs, we immunostained the femoral bone marrow for Sca-1, which, as discussed previously, identifies more committed murine HSPCs. Both PKH26 and miRFP703 fluorescent puncta were extensively colocalized with the $Sca\text{-}1^+$ marrow cells of the CHEV hybrid-treated mice, demonstrating that plasmid delivery to HSPCs using the loaded hybrid particles is feasible (Figure 7D). Upon further magnification, we also found extensive localization of strong miRFP fluorescence on the periphery of the blood vessels in the bone marrow vasculature of CHEV hybrid-treated mice, but to a lesser extent for liposome-treated mice (Figure 7E). The periphery of bone-marrow blood vessels is an HSPC-rich region (Itkin et al., 2016). We also found PKH26 fluorescence localized to these same vessel walls in the CHEV hybrid-treated marrow, although much less pronounced than for miRFP fluorescence (Figure 7E).

We also immunostained other tissues in addition to the femoral bone marrow, and we detected miRFP expression and some colocalization to other $Sca\text{-}1^+$ cells in spleen and kidneys, albeit to a much lesser degree than the marrow (Supplementary Figure S5). Given the data of Figure 7C, we observed miRFP expression in $CD41^+$ cells within the femurs but did not observe any distinct localization patterns in the other tissues like what we observed with $Sca\text{-}1^+$ cells (Supplementary Figure S6).

Taken together, these data suggest that the CHEV hybrids retain their tropism to HSPCs *in vivo*, further demonstrating their potential versatility as a tailorable vehicle for targeted cargo delivery to HSPCs.

4 Discussion

In these studies, we showed that huMkEVs robustly spur megakaryopoiesis of murine HSPCs *in vitro* and *in vivo* and can ultimately spur *de novo* biosynthesis of platelets. As we have previously suggested, given that they can be stored frozen, huMkEVs may offer a robust alternative to platelet transfusions for treating thrombocytopenias which affect millions of individuals worldwide (Escobar et al., 2020). Platelets for transfusion therapy are prepared from collected donor blood and is an expensive product in limited supply due to the short shelf life as platelets cannot be frozen (Huish et al., 2019; Sireis et al., 2011). While there have been improvements in the handling and shelf life, banked platelets can only be stored for a maximum of 5 days and extended storage may reduce their overall clotting strength (Huish et al., 2019; Sireis et al., 2011). By using the immunocompromised NSG strain, we were able to effectively probe these murine responses to huMkEVs with limited interference from the murine immune system, and thus better elucidate the phenotypic response to the huMkEV treatment. We have demonstrated that huMkEVs exhibit strong tropism for murine and human HSPCs, and intravenously administered huMkEVs home to the HSPC-rich bone marrow and promote megakaryopoiesis in NSG mice in relatively short timescales due to endogenous phenotype-determining cargo contained within the huMkEVs (Belliveau and Papoutsakis, 2022; C. Y; Kao et al., 2022). When coupling the effectiveness of huMkEV-induced megakaryopoiesis and the relative resilience to storage conditions, huMkEVs could be a valuable therapeutic for patients suffering from thrombocytopenia.

We have also shown that huMkEVs can be modified to carry exogenous cargo, thus laying the groundwork for a naturally-derived drug delivery vehicle for normally hard-to-transfect HSPCs (Yu et al., 2016). We deployed two methods for exogenously loading huMkEVs and CHRF EVs with plasmid DNA: either by direct electroporation or using hybridization of these EVs with liposomes. While we were able to demonstrate the effectiveness of using these exogenous loading methods to create an EV-based vehicle for HSPC-specific functional cargo delivery, this concept can be further optimized for improved delivery efficiency to HSPCs and other cells. First, we selected an arbitrary dose of loaded hybrid particles to intravenously deliver to the NSG mice as an initial proof of concept. The data suggest that 10 to 20-fold higher dosages might provide a stronger measure of the potential of this delivery system. To improve targeting of HSPCs, EVs could be generated from cells overexpressing certain surface proteins and moieties, e.g., ICAM-1 or MAC-1 in the case of HSPCs and may facilitate improved uptake into the target cell (Bronshtein et al., 2011; Das et al., 2023; Jiang et al., 2017). Other surface molecules, such as polyethylene glycol (PEG), can be used to 'PEGylate' the surface of liposomes and other particles and promote extended circulation of the administered PEGylated therapeutic *in vivo* (de Jong et al., 2019; Harris et al., 2019; Krishnamurthy et al., 2019; Pachauri et al., 2015). Further modifications to the

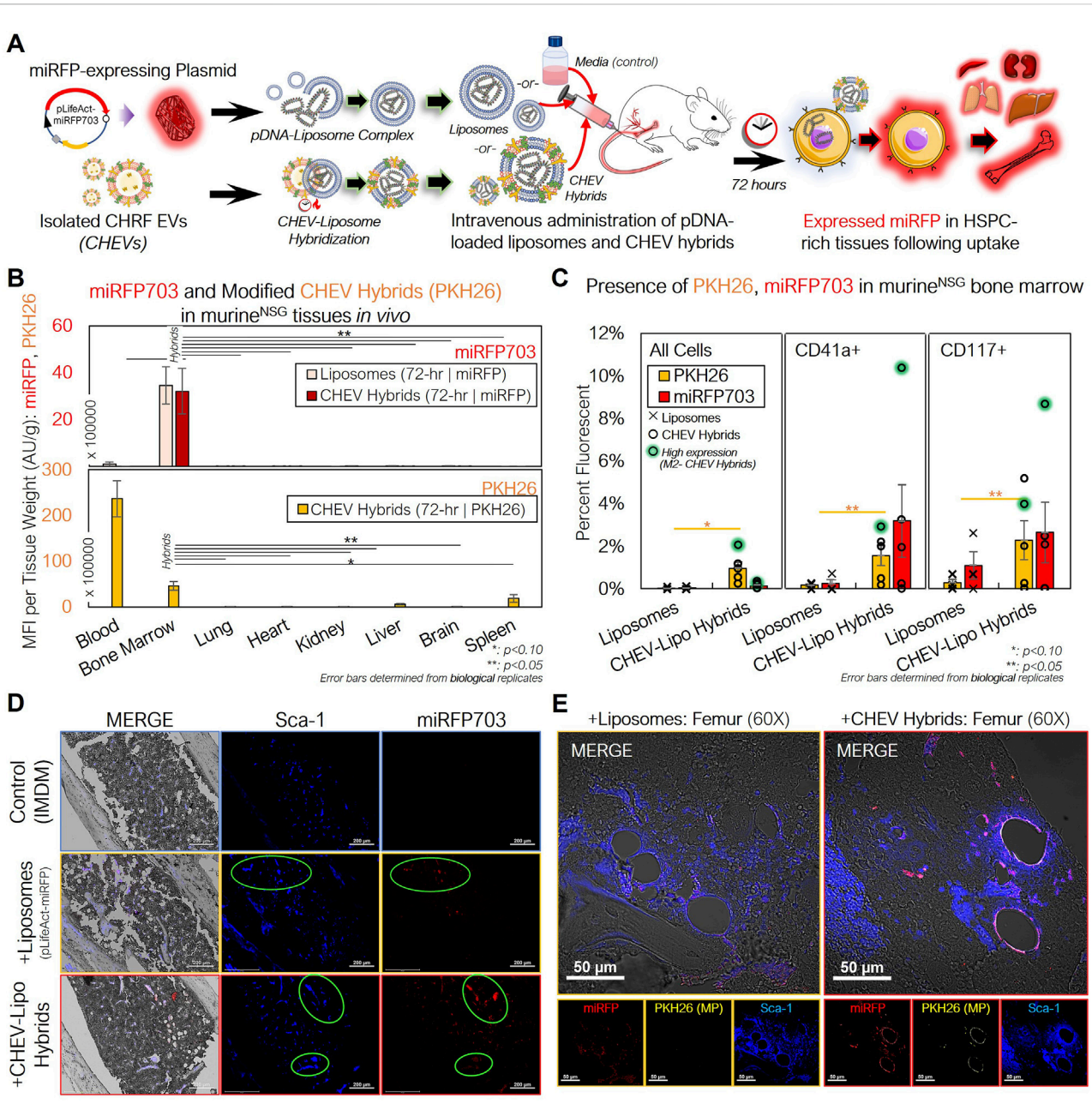

FIGURE 7
pDNA-loaded CHEV-liposome hybrids can be used for efficient HSPC-specific nucleic acid delivery *in vivo*. **(A)** Experimental schema for preparing pLifeAct-miRFP703-loaded liposomes or CHEV-liposome hybrids for targeted pDNA delivery to murine HSPCs *in vivo*. **(B)** NSG mice were intravenously administered either 10 µg of miRFP703-expressing pDNA complexed with liposomes ($n = 3$) or pDNA-loaded liposomes further hybridized with ~50 x 10^6 PKH26-labeled CHEVs (CHEV hybrids; n = 5), and various tissues were excised, homogenized, and assessed for PKH26 (gold) and miRFP703 (red; top) fluorescence and PKH26 biodistribution (CHEVs-only; bottom) 72-h post particle intravenous delivery. **(C)** Flushed RBC-depleted marrow cells from mice treated with either pDNA-loaded liposomes (pLifeAct-miRFP703) or CHEV hybrids and a media (IMDM)-treated control were immunostained for $CD117^+$ murine HSPCs and $CD41a^+$ murine Mk cells and screened for miRFP703 expression and CHEV hybrid localization (PKH26-fluorescent) via flow cytometry. High miRFP703-expressing mouse indicated in green. **(D)** Femurs from 72-hour-treated mice were fixed (10% neutral-buffered formalin), sectioned, immunostained and assessed for structure (gray- DIC) and presence of $Sca\text{-}1^+$ cells (blue), miRFP703 expression (red) and PKH26 arising from administered CHEV-liposome hybrids. Colocalization of murine HSPCs and miRFP703 indicated with light green circles. Scale bars: 200-µm. **(E)** Magnified image of sectioned femurs from liposome- and CHEV-liposome hybrid-treated mice showing extensive miRFP expression and colocalization of expression with $Sca\text{-}1^+$ HSPCs. Colocalization of $Sca\text{-}1^+$ and miRFP703 shown as lavender in the merged image. Scale bars: 50-µm. *:$p < 0.1$:**: $p < 0.05$, ***: $p < 0.01$, ****: $p < 0.001$. Analysis of Variance (ANOVA) was used for statistical comparisons for all animal experiments.

payload and vesicle surface, such as cell-penetrating peptides, can also improve endosomal escape of the cargo, further improving intracellular trafficking of the delivered cargo (Lonn et al., 2016; Varkouhi et al., 2011). Finally, the composition of the EV-liposome mix could be further altered to encapsulate a broader range of cargo, including larger plasmids, RNA, and proteins. Thus, both native and engineered huMkEVs have significant promise as a robust therapeutic for a broad spectrum of hematological diseases.

In conclusion, we have demonstrated that huMkEVs and huMkEV-like CHEVs natively target and deliver functional cargo to HSPCs, which can ultimately translate to a modified HSPC phenotype. As HSPCs differentiate and commit to other blood cell lineages, huMkEVs and CHEVs could facilitate targeted delivery of therapeutics to HSPCs to treat various hematological diseases.

Data availability statement

The original contributions presented in the study are included in the article/Supplementary Material, further inquiries can be directed to the corresponding author.

Ethics statement

Ethical approval was not required for the studies on humans in accordance with the local legislation and institutional requirements because only commercially available established cell lines were used. The animal study was approved by the Mice were handled humanely under IACUC approved Animal Use Protocol #1290. The study was conducted in accordance with the local legislation and institutional requirements.

Author contributions

SD: Conceptualization, Data curation, Formal Analysis, Investigation, Methodology, Resources, Visualization, Writing–original draft, Writing–review and editing. WT: Data curation, Investigation, Writing–review and editing. EP: Conceptualization, Data curation, Formal Analysis, Funding acquisition, Investigation, Methodology, Project administration, Resources, Supervision, Validation, Visualization, Writing–original draft, Writing–review and editing.

Funding

The author(s) declare that financial support was received for the research, authorship, and/or publication of this article. CSL Behring through the Science Center (https://sciencecenter.org) (EP). National Science Foundation (NSF) grant CBET-1804741 (EP). Microscopy equipment (Carl Zeiss LSM880 confocal microscope) was acquired with a shared instrumentation grant (S10 OD016361) and access was supported by the NIH-NIGMS (P20 GM103446), the US NSF (IIA-1301765) and the State of Delaware. Use of the University of Delaware Animal Laboratory and Histology Core Facility were supported by the DCMR COBRE program, with a grant from the National Institute of General Medical Sciences and from the National Institutes of Health–NIH-NIGMS COBRE (P20 GM139760).

Acknowledgments

We would like to thank Christina Stinger from the University of Delaware Office of Laboratory Medicine for assistance with the animal experiments. We would also like to thank the members of the Nemours Histology Core Facility and Charles Riley from the Delaware Biotechnology Institute for their assistance with the tissue sectioning and immunostaining. Finally, we would like to thank Shannon Modla and Jean Ross and other members from the Bioimaging Center at the Delaware Biotechnology Institute for their assistance with transmission electron microscopy.

Conflict of interest

The authors declare that the research was conducted in the absence of any commercial or financial relationships that could be construed as a potential conflict of interest.

Publisher's note

Supplementary material

The Supplementary Material for this article can be found online at: https://www.frontiersin.org/articles/10.3389/fbioe.2024.1435228/full#supplementary-material

References

Belliveau, J., and Papoutsakis, E. T. (2022). Extracellular vesicles facilitate large-scale dynamic exchange of proteins and RNA among cultured Chinese hamster ovary and human cells. *Biotechnol. Bioeng.* 119 (5), 1222–1238. doi:10.1002/bit.28053

Belliveau, J., and Papoutsakis, E. T. (2023). The microRNomes of Chinese hamster ovary (CHO) cells and their extracellular vesicles, and how they respond to osmotic and ammonia stress. *Biotechnol. Bioeng.* 120, 2700–2716. doi:10.1002/bit.28356

Blake, P. G., Madrenas, J., and Halloran, P. F. (1993). Ly-6 in kidney is widely expressed on tubular epithelium and vascular endothelium and is up-regulated by interferon gamma. *J. Am. Soc. Nephrol.* 4 (5), 1140–1150. doi:10.1681/ASN.V451140

Brehm, M. A., Kenney, L. L., Wiles, M. V., Low, B. E., Tisch, R. M., Burzenski, L., et al. (2019). Lack of acute xenogeneic graft-versus-host disease, but retention of T-cell function following engraftment of human peripheral blood mononuclear cells in NSG mice deficient in MHC class I and II expression. *FASEB J.* 33 (3), 3137–3151. doi:10.1096/fj.201800636R

Bronshtein, T., Toledano, N., Danino, D., Pollack, S., and Machluf, M. (2011). Cell derived liposomes expressing CCR5 as a new targeted drug-delivery system for HIV infected cells. *J. Control. Release* 151 (2), 139–148.

Cao, X. Q., Shores, E. W., Huli, J., Anver, M. R., Kelsall, B. L., Russell, S. M., et al. (1995). Defective lymphoid development in mice lacking expression of the common cytokine receptor-gamma chain. *Immunity* 2 (3), 223–238. doi:10.1016/1074-7613(95)90047-0

Cray, C., Keane, R. W., Malek, T. R., and Levy, R. B. (1990). Regulation and selective expression of Ly-6A/E, a lymphocyte activation molecule, in the central nervous system. *Brain Res. Mol. Brain Res.* 8 (1), 9–15. doi:10.1016/0169-328x(90)90003-v

Cuenca-Zamora, E. J., Ferrer-Marin, F., Rivera, J., and Teruel-Montoya, R. (2019). Tubulin in platelets: when the shape matters. *Int. J. Mol. Sci.* 20 (14), 3484. doi:10.3390/ijms20143484

Das, S., Harris, J. C., Winter, E. J., Kao, C. Y., Day, E. S., and Papoutsakis, E. T. (2023). Megakaryocyte membrane-wrapped nanoparticles for targeted cargo delivery to hematopoietic stem and progenitor cells. *Bioeng. and Transl. Med.* 8 (3), e10456. doi:10.1002/btm2.10456

de Jong, O. G., Kooijmans, S. A. A., Murphy, D. E., Jiang, L., Evers, M. J. W., Sluijter, J. P. G., et al. (2019). Drug delivery with extracellular vesicles: from imagination to innovation. *Acc. Chem. Res.* 52 (7), 1761–1770. doi:10.1021/acs.accounts.9b00109

Escobar, C., Kao, C. Y., Das, S., and Papoutsakis, E. T. (2020). Human megakaryocytic microparticles induce *de novo* platelet biogenesis in a wild-type murine model. *Blood Adv.* 4 (5), 804–814. doi:10.1182/bloodadvances.2019000753

Estes, S., Konstantinov, K., and Young, J. D. (2022). Manufactured extracellular vesicles as human therapeutics: challenges, advances, and opportunities. *Curr. Opin. Biotechnol.* 77, 102776. doi:10.1016/j.copbio.2022.102776

Flaumenhaft, R., Dilks, J. R., Richardson, J., Alden, E., Patel-Hett, S. R., Battinelli, E., et al. (2009). Megakaryocyte-derived microparticles: direct visualization and distinction from platelet-derived microparticles. *Blood* 113 (5), 1112–1121. doi:10.1182/blood-2008-06-163832

Forteza-Genestra, M. A., Antich-Rossello, M., Ortega, F. G., Ramis-Munar, G., Calvo, J., Gaya, A., et al. (2021). Labeling of extracellular vesicles for monitoring migration and uptake in cartilage explants. *J. Vis. Exp.* 176. doi:10.3791/62780

Fugman, D. A., Witte, D. P., Jones, C. L., Aronow, B. J., and Lieberman, M. A. (1990). *In vitro* establishment and characterization of a human megakaryoblastic cell line. *Blood* 75 (6), 1252–1261. doi:10.1182/blood.v75.6.1252.bloodjournal7561252

Fuhrken, P. G., Chen, C., Miller, W. A., and Papoutsakis, E. T. (2007). Comparative, genome-scale transcriptional analysis of CHRF-288-11 and primary human megakaryocytic cell cultures provides novel insights into lineage-specific differentiation. *Exp. Hematol.* 35 (3), 476–489.e23. doi:10.1016/j.exphem.2006.10.017

Harris, J. C., Scully, M. A., and Day, E. S. (2019). Cancer Cell Membrane-Coated Nanoparticles for Cancer Management. *Cancers (Basel)* 11 (12), 1836.

Holmes, C., and Stanford, W. L. (2007). Concise review: stem cell antigen-1: expression, function, and enigma. *Stem Cells* 25 (6), 1339–1347. doi:10.1634/stemcells.2006-0644

Huish, S., Green, L., Curnow, E., Wiltshire, M., and Cardigan, R. (2019). Effect of storage of plasma in the presence of red blood cells and platelets: re-evaluating the shelf life of whole blood. *Transfusion* 59 (11), 3468–3477.

Itkin, T., Gur-Cohen, S., Spencer, J. A., Schajnovitz, A., Ramasamy, S. K., Kusumbe, A. P., et al. (2016). Distinct bone marrow blood vessels differentially regulate haematopoiesis. *Nature* 532 (7599), 323–328. doi:10.1038/nature17624

Jiang, J., Kao, C. Y., and Papoutsakis, E. T. (2017). How do megakaryocytic microparticles target and deliver cargo to alter the fate of hematopoietic stem cells? *J. Control Release* 247, 1–18. doi:10.1016/j.jconrel.2016.12.021

Jiang, J., Woulfe, D. S., and Papoutsakis, E. T. (2014). Shear enhances thrombopoiesis and formation of microparticles that induce megakaryocytic differentiation of stem cells. *Blood* 124 (13), 2094–2103. doi:10.1182/blood-2014-01-547927

Jindal, N., Minhas, G., Prabhakar, S., and Anand, A. (2014). Characterization of Lin-ve CD34 and CD117 cell population reveals an increased expression in bone marrow derived stem cells. *Curr. Neurovasc Res.* 11 (1), 68–74. doi:10.2174/1567202610666131209110035

Kao, C.-Y., Jiang, J., Thompson, W., and Papoutsakis, E. T. (2022). miR-486-5p and miR-22-3p enable megakaryocytic differentiation of hematopoietic stem and progenitor cells without thrombopoietin. *Int. J. Mol. Sci.* 23 (10), 5355. doi:10.3390/ijms23105355

Kao, C.-Y., and Papoutsakis, E. T. (2018). Engineering human megakaryocytic microparticles for targeted delivery of nucleic acids to hematopoietic stem and progenitor cells. *Sci. Adv.* 4 (11), eaau6762. doi:10.1126/sciadv.aau6762

Krishnamurthy, S., Muthukumaran, P., Jayakumar, M. K. G., Lisse, D., Masurkar, N. D., Xu, C., et al. (2019). Surface protein engineering increases the circulation time of a cell membrane-based nanotherapeutic. *Nanomedicine* 18, 169–178.

Konkle, B. A., Schuster, S. J., Kelly, M. D., Harjes, K., Hassett, D. E., Bohrer, M., et al. (1992). Plasminogen activator inhibitor-1 messenger RNA expression is induced in rat hepatocytes *in vivo* by dexamethasone. *Blood* 79 (10), 2636–2642. doi:10.1182/blood.v79.10.2636.2636

Li, L., He, D., Guo, Q., Zhang, Z., Ru, D., Wang, L., et al. (2022). Exosome-liposome hybrid nanoparticle codelivery of TP and miR497 conspicuously overcomes chemoresistant ovarian cancer. *J. Nanobiotechnology* 20 (1), 50. doi:10.1186/s12951-022-01264-5

Lin, Y., Wu, J., Gu, W., Huang, Y., Tong, Z., Huang, L., et al. (2018). Exosome-liposome hybrid nanoparticles deliver CRISPR/Cas9 system in MSCs. *Adv. Sci. (Weinh)* 5 (4), 1700611. doi:10.1002/advs.201700611

Lindsey, S., and Papoutsakis, E. T. (2011). The aryl hydrocarbon receptor (AHR) transcription factor regulates megakaryocytic polyploidization. *Br. J. Haematol.* 152 (4), 469–484. doi:10.1111/j.1365-2141.2010.08548.x

Lonn, P., Kacsinta, A. D., Cui, X. S., Hamil, A. S., Kaulich, M., Gogoi, K., et al. (2016). Enhancing Endosomal Escape for Intracellular Delivery of Macromolecular Biologic Therapeutics. *Sci. Rep.* 6, 32301.

Madaan, A., Verma, R., Singh, A. T., Jain, S. K., and Jaggi, M. (2014). A stepwise procedure for isolation of murine bone marrow and generation of dendritic cells. *J. Biol. Methods* 1 (1), 1. doi:10.14440/jbm.2014.12

McGrath, R. T., McRae, E., Smith, O. P., and O'Donnell, J. S. (2010). Platelet von Willebrand factor--structure, function and biological importance. *Br. J. Haematol.* 148 (6), 834–843. doi:10.1111/j.1365-2141.2009.08052.x

Nadri, S., Soleimani, M., Hosseni, R. H., Massumi, M., Atashi, A., and Izadpanah, R. (2007). An efficient method for isolation of murine bone marrow mesenchymal stem cells. *Int. J. Dev. Biol.* 51 (8), 723–729. doi:10.1387/ijdb.072352ns

Nienhuis, A. W. (2013). Development of gene therapy for blood disorders: an update. *Blood* 122 (9), 1556–1564. doi:10.1182/blood-2013-04-453209

Osborn, M. J., Belanto, J. J., Tolar, J., and Voytas, D. F. (2016). Gene editing and its application for hematological diseases. *Int. J. Hematol.* 104 (1), 18–28. doi:10.1007/s12185-016-2017-z

Pachauri, M., Gupta, E. D., and Ghosh, P. C. (2015). Piperine loaded PEG-PLGA nanoparticles: Preparation, characterization and targeted delivery for adjuvant breast cancer chemotherapy. *J. Drug Deliv. Sci. Technol.* 29, 269–282.

Panuganti, S., Schlinker, A. C., Lindholm, P. F., Papoutsakis, E. T., and Miller, W. M. (2013). Three-stage *ex vivo* expansion of high-ploidy megakaryocytic cells: toward large-scale platelet production. *Tissue Eng. Part A* 19 (7-8), 998–1014. doi:10.1089/ten.TEA.2011.0111

Puzar Dominkus, P., Stenovec, M., Sitar, S., Lasic, E., Zorec, R., Plemenitas, A., et al. (2018). PKH26 labeling of extracellular vesicles: characterization and cellular internalization of contaminating PKH26 nanoparticles. *Biochim. Biophys. Acta Biomembr.* 1860 (6), 1350–1361. doi:10.1016/j.bbamem.2018.03.013

Ravid, K., Lu, J., Zimmet, J. M., and Jones, M. R. (2002). Roads to polyploidy: the megakaryocyte example. *J. Cell Physiol.* 190 (1), 7–20. doi:10.1002/jcp.10035

Reya, T. (1996). The role of interleukin-2 in hematopoiesis. PhD Thesis. Philadelphia: Univ. of Pennsylvania.

Rodriguez, P. L., Harada, T., Christian, D. A., Pantano, D. A., Tsai, R. K., and Discher, D. E. (2013). Minimal "Self" peptides that inhibit phagocytic clearance and enhance delivery of nanoparticles. *Science* 339 (6122), 971–975. doi:10.1126/science.1229568

Sadler, J. E. (2005). New concepts in von Willebrand disease. *Annu. Rev. Med.* 56, 173–191. doi:10.1146/annurev.med.56.082103.104713

Saito, Y., Shultz, L. D., and Ishikawa, F. (2020). Understanding normal and malignant human hematopoiesis using next-generation humanized mice. *Trends Immunol.* 41 (8), 706–720. doi:10.1016/j.it.2020.06.004

Sireis, W., Ruster, B., Daiss, C., Hourfar, M. K., Capalbo, G., Pfeiffer, H. U., et al. (2011). Extension of platelet shelf life from 4 to 5 days by implementation of a new screening strategy in Germany. *Vox Sang* 101 (3), 191–199.

Serreze, D. V., Gaedeke, J. W., and Leiter, E. H. (1993). Hematopoietic stem-cell defects underlying abnormal macrophage development and maturation in NOD/Lt mice: defective regulation of cytokine receptors and protein kinase C. *Proc. Natl. Acad. Sci. U. S. A.* 90 (20), 9625–9629. doi:10.1073/pnas.90.20.9625

Shcherbakova, D. M., Baloban, M., Emelyanov, A. V., Brenowitz, M., Guo, P., and Verkhusha, V. V. (2016). Bright monomeric near-infrared fluorescent proteins as tags and biosensors for multiscale imaging. *Nat. Commun.* 7, 12405. doi:10.1038/ncomms12405

Strowig, T., Rongvaux, A., Rathinam, C., Takizawa, H., Borsotti, C., Philbrick, W., et al. (2011). Transgenic expression of human signal regulatory protein alpha in $Rag2^{-/-}\gamma_c^{-/-}$mice improves engraftment of human hematopoietic cells in humanized mice. *Proc. Natl. Acad. Sci. U. S. A.* 108 (32), 13218–13223. doi:10.1073/pnas.1109769108

Thery, C., Witwer, K. W., Aikawa, E., Alcaraz, M. J., Anderson, J. D., Andriantsitohaina, R., et al. (2018). Minimal information for studies of extracellular vesicles 2018 (MISEV2018): a position statement of the International Society for Extracellular Vesicles and update of the MISEV2014 guidelines. *J. Extracell. Vesicles* 7 (1), 1535750. doi:10.1080/20013078.2018.1535750

Thompson, W., and Papoutsakis, E. T. (2023a). The role of biomechanical stress in extracellular vesicle formation, composition and activity. *Biotechnol. Adv.* 66, 108158. doi:10.1016/j.biotechadv.2023.108158

Thompson, W., and Papoutsakis, E. T. (2023b). Similar but distinct: the impact of biomechanical forces and culture age on the production, cargo loading, and biological efficacy of human megakaryocytic extracellular vesicles for applications in cell and gene therapies. *Bioeng. and Transl. Med.* 8, e10563. doi:10.1002/btm2.10563

Vanderijn, M., Heimfeld, S., Spangrude, G. J., and Weissman, I. L. (1989). Mouse hematopoietic stem-cell antigen sca-1 is a member of the ly-6 antigen family. *Proc. Natl. Acad. Sci. U S A* 86 (12), 4634–4638. doi:10.1073/pnas.86.12.4634

Varkouhi, A. K., Scholte, G., Storm, G., and Haisma, H. J. (2011). Endosomal escape pathways for delivery of biologicals. *J. Control. Release* 151 (3), 220–228.

Visnjic, D., Kalajzic, Z., Rowe, D. W., Katavic, V., Lorenzo, J., and Aguila, H. L. (2004). Hematopoiesis is severely altered in mice with an induced osteoblast deficiency. *Blood* 103 (9), 3258–3264. doi:10.1182/blood-2003-11-4011

Wang, Y., Hayes, V., Jarocha, D., Sim, X., Harper, D. C., Fuentes, R., et al. (2015). Comparative analysis of human *ex vivo*-generated platelets vs megakaryocyte-generated platelets in mice: a cautionary tale. *Blood* 125 (23), 3627–3636. doi:10.1182/blood-2014-08-593053

Yu, K. R., Natanson, H., and Dunbar, C. E. (2016). Gene editing of human hematopoietic stem and progenitor cells: promise and potential hurdles. *Hum. Gene Ther.* 27 (10), 729–740. doi:10.1089/hum.2016.107

Yurino, A., Takenaka, K., Yamauchi, T., Nunomura, T., Uehara, Y., Jinnouchi, F., et al. (2016). Enhanced reconstitution of human erythropoiesis and thrombopoiesis in an immunodeficient mouse model with kit(wv) mutations. *Stem Cell Rep.* 7 (3), 425–438. doi:10.1016/j.stemcr.2016.07.002